

Polarization control mechanisms in vectorial bistable lasers for one-frequency systems

G. Ropars and A. Le Floch

Laboratoire d'Electronique Quantique, Physique des Lasers, Université de Rennes I, F-35042 Rennes CEDEX, France

R. Le Naour

Laboratoire d'Electronique Quantique, Université de Nantes, F-44072 Nantes CEDEX, France

(Received 16 October 1991; revised manuscript received 3 February 1992)

The basic mechanisms of the polarization switching in vectorial bistable lasers are studied both theoretically and experimentally versus internal parameters. In particular, by scanning the frequency of a gas laser with two linearly polarized eigenstates, two quite different flipping processes with hysteresis occur according to the linear-phase-anisotropy value of the cavity. Indeed, when the anisotropy increases, *rotation* and *inhibition* mechanisms appear successively. The variations of the hysteresis loop for different anisotropy and excitation values are theoretically found to be opposed in the two processes. Additional evolutions of the polarization, such as multiple switchings in the inhibition mechanism and "hybrid" hysteresis loops, are predicted. The experiments, essentially performed on a monomode 3.39- μm $^3\text{He-}^{20}\text{Ne}$ laser containing an adjustable linear phase anisotropy, confirm the existence of the two processes and their corresponding properties. These processes may also occur in other quasi-isotropic lasers versus other internal parameters, such as, for instance, the injection current in semiconductor lasers. In this case the TE and TM modes flip only in the inhibition mechanism when the bistability conditions are satisfied. The knowledge of the basic flipping mechanisms in the laser itself enables us to understand and realize the external optical-polarization control by an anisotropic feedback (one-frequency systems). *Induced-rotation* and *induced-inhibition* mechanisms are then theoretically predicted and experimentally verified. Sensitive optical gates are realized by varying the feedback phase in both processes.

PACS number(s): 42.65.Pc

I. INTRODUCTION

Optical bistability is a rapidly expanding field of current research because of its applications to all-optical logic [1,2] and because of the interesting phenomena it encompasses [3]. Most of the classical bistable devices are passive and scalar [3] with the incident intensity as the fundamental parameter. Bistability, however, was first studied in active systems, i.e., in lasers, by Lamb and co-workers [4]. Indeed, Lamb noted the close connection between van der Pol's work [5] developed on electrical oscillators and a two-longitudinal-mode laser with a fixed linear polarization. In his analysis he introduces a mode-coupling constant C that fixes the behavior of the two oscillating modes. On one hand, for a low coupling-constant value, i.e., $C < 1$, the two longitudinal modes with the same polarization can oscillate simultaneously at two different frequencies. On the other hand, for a high coupling-constant value, i.e., $C > 1$, there can be a mode inhibition mechanism with hysteresis when the frequency is scanned. Only a few experiments have been performed on the competition between two longitudinal modes because its analysis needs a separation in frequency of the two modes [6]. In contrast to the scalar bistability, vectorial bistability between two eigenstates of a single-mode cavity seems more attractive because the polarization can be simply isolated by a polarizer. Polarization bistability was observed in the earlier years of gas-laser physics [7–12]. Unfortunately, the dynamic of this bistability was

of great complexity from both the experimental and theoretical points of view. In particular, the possible changes of the polarization switching processes due to a variation of the cavity phase anisotropy, for instance, were not investigated. More recently, the spatial representation of the "generalized potentials" associated with the two eigenstates of a quasi-isotropic monomode laser in the frame of the Landau theory [13] predicted two different types of first-order phase transitions according to the phase-anisotropy values [14]. The system may switch from one linearly polarized eigenstate, for instance, to the other one either by a *rotation* of the electric field or by an *inhibition* mechanism. In this latter mechanism one eigenstate switches off while simultaneously the other one switches on at a different frequency. A polarizer allows one to distinguish clearly between these two processes. Indeed, if it is rotated at $\pm 45^\circ$ from an eigenstate only the rotation mechanism gives an extinction (dip) or a doubling (peak) of the transmitted intensity during the eigenstates flips. It has been shown that when the frequency is scanned, the two processes occur in quasi-isotropic $^3\text{He-}^{20}\text{Ne}$ gas lasers depending on the value of an internal adjustable linear birefringence [14]. Control of the polarization by an external anisotropic feedback [15–18] including the spurious reflection from the window of a detector has also been realized. However, as the nature of the polarization flipping was not isolated in these last works, this prevented a complete interpretation of the observations.

The aim of the first part of this paper is to give a detailed description of the properties of the basic polarization flipping mechanisms occurring in quasi-isotropic lasers. This will then allow us to give insights into the polarization control by anisotropic feedbacks [19]. In Sec. II we discuss theoretically and verify experimentally the polarization switching processes occurring in a gas laser when an internal parameter such as the laser frequency for instance is varied. The evolutions of the hysteresis loops for different phase anisotropy and laser excitation values are given. The existence of multiple switchings in the inhibition mechanism will also be investigated. We also wonder whether it is possible to obtain one of each mechanism for a given particular hysteresis loop, i.e., to realize a hybrid hysteresis loop. The basic flipping mechanisms may also occur in other quasi-isotropic lasers when another internal parameter is varied. As an example, we will consider the flip between TE and TM modes in a semiconductor laser [20,21]. The complete knowledge of the basic mechanisms then allows one to investigate in Sec. III a vectorial control by anisotropic feedbacks, i.e., in one-frequency systems.

II. THE BASIC MECHANISMS OF THE POLARIZATION FLIP

A. Prediction of the rotation and of the inhibition mechanisms

Let us first recall that for a monomode laser with a fixed linear polarization, the time evolution of the field amplitude E near threshold is written according to Lamb's model [4]

$$\dot{E} = E(\alpha - \beta E^2), \quad (1)$$

where the temporal net gain α and the self-saturation β depend on the laser frequency ν . We recall also that as in Landau's theory of structural phase transitions [13], the steady-state solution of Eq. (1) can be associated with a potential [22–24]

$$V(E) = -\frac{1}{2}\alpha E^2 + \frac{1}{4}\beta E^4, \quad (2)$$

which will be generalized later. This type of potential is adapted to lasers with strong anisotropies, i.e., with an intracavity element that selects one state of linear polarization of the electromagnetic field by strongly increasing the losses for the other state. A question then arises: what is the behavior of the polarization when the anisotropies become weak, but remain well known and adjustable? To answer this question let us consider a quasi-isotropic monomode gas laser containing an adjustable linear phase anisotropy $\Delta\Phi_{xy}$ as shown in Fig. 1(a). This linear phase anisotropy can be obtained by a stressed plate inserted in the cavity. The determination of the eigenstates is performed by the resolution of the resonance condition $M\mathbf{E} = \Lambda\mathbf{E}$, where M is the 2×2 Jones matrix [25] for one round trip in the cavity and \mathbf{E} is the electric-field vector. The eigenvectors of matrix M contain the intensities and polarizations of the two eigenstates and the associated eigenvalues Λ lead to the

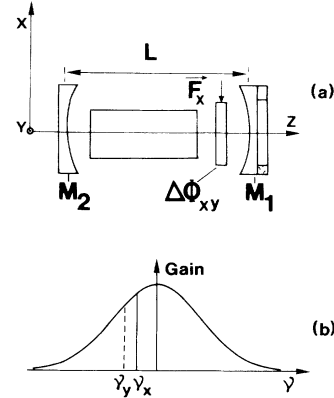


FIG. 1. (a) General setup for the polarization flipping analysis. $\Delta\Phi_{xy}$ is a linear phase anisotropy introduced by a stressed plate. (b) Position of the eigenstates frequencies within the Doppler profile for a given laser cavity length.

knowledge of their eigenfrequencies [26]. In the following we will deal with an active medium which oscillates on a preferentially linearly polarized emission line as, for instance, the $3.39\text{-}\mu\text{m}$ line (a $J=1 \rightarrow J=2$ transition) [8–10]. Then the eigenstates polarizations depend only on the optical elements of the cavity and are along the x and the y axes of the phase anisotropy. The two linear eigenstates have slightly different eigenfrequencies whose difference is

$$\Delta\nu_{xy} = \nu_x - \nu_y = \frac{c}{2L} \frac{\Delta\Phi_{xy}}{\pi}, \quad (3)$$

where L is the cavity length and c is the velocity of light. Once these eigenstates are defined, one must investigate their possible oscillating regime. If a stress is applied along the x axis, the optical path for an electric field polarized along this axis is shorter than that for a field polarized along the y axis implying $\nu_x > \nu_y$. One can then predict that the eigenstate which reaches first the threshold when the frequency increases (decreases) is always the x (y) eigenstate [Fig. 1(b)]. Furthermore, as the gain of the x and the y eigenstates is different according to their position within the Doppler frequency profile, either the x or the y eigenstate is favored. Polarization flipping can then occur when the frequency is scanned and this behavior will be confirmed experimentally for different $\Delta\Phi_{xy}$ values. Let us see now how the phase-anisotropy value governs the nature of the flipping process.

We begin by the case of small $\Delta\Phi_{xy}$ phase-anisotropy values, i.e., for close eigenstates frequencies. It is well known that in such case a locking phenomenon occurs between the two nonlinear oscillators as, for example, between two electrical oscillators [5], between the σ components in a Zeeman laser [27], or between the two counterpropagating waves in a ring laser [28]. Then during the flip there is a single oscillator $\mathbf{E} = \mathbf{E}_x + \mathbf{E}_y$ whose polarization may rotate in the E_x - E_y plane and one may ask what is the potential associated with this system. During the flip from x to y , for instance, the electric-field fre-

quency ν is shifted from ν_x to ν_y . None of the E_x and E_y field components is exactly at cavity resonance during the flip. This results in a loss term [29] noted $\Delta p(\theta)$ which depends on the rotation angle θ of the polarization from the x axis. An evaluation of these losses is obtained in Appendix A, where we find

$$\Delta p(\theta) \approx 8\Delta\Phi_{xy}^2 [\theta^2 \cos^2\theta + (\pi/2 - \theta)^2 \sin^2\theta] / \pi^2. \quad (4)$$

In Fig. 2 we have represented $\Delta p(\theta)$ for different $\Delta\Phi_{xy}$ values. We notice a quadratic dependence on $\Delta\Phi_{xy}$ and verify that the losses cancel for $\theta=0$ and $\theta=\pi/2$ positions for which the laser is at resonance. For $\theta=\pi/4$ the losses are maximum and take the value $\Delta p(\pi/4) = \Delta\Phi_{xy}^2/2$. This allows us to give now a first analysis of the rotation mechanism. The potential $V(E, \theta)$ associated with the system can be deduced from Eq. (2) by including the extra losses $\Delta p(\theta)$ and a frequency shift with θ . The net gain for the field amplitude becomes

$$\alpha(\theta) = \alpha_0 \exp \left[- \left[\frac{\nu(\theta) - \nu_0}{\Delta\nu_D/2} \right]^2 \right] - p - \frac{c}{2L} \Delta p(\theta), \quad (5)$$

where α_0 is the unsaturated gain coefficient for the field amplitude at the resonance frequency of the atomic transition ν_0 , p are the average cavity losses per second, and $\Delta\nu_D$ is the full Doppler width at $1/e$. The self-saturation β is written as

$$\beta(\theta) = \beta_0 \left[1 + \frac{\gamma^2}{\gamma^2 + [\nu(\theta) - \nu_0]^2} \right] \times \exp \left[- \left[\frac{\nu(\theta) - \nu_0}{\Delta\nu_D/2} \right]^2 \right], \quad (6)$$

where β_0 characterizes the self-saturation at line center and γ is the homogeneous width of the transition [half width at half maximum (HWHM)]. We have chosen for simplification a linear variation of ν with θ . As we shall see it is sufficient to give for a low anisotropy value and for given eigenstates frequencies a representation of the potential $V(E, \theta)$. In Fig. 3 we can follow the deformation of such a potential with the laser frequency. Let us

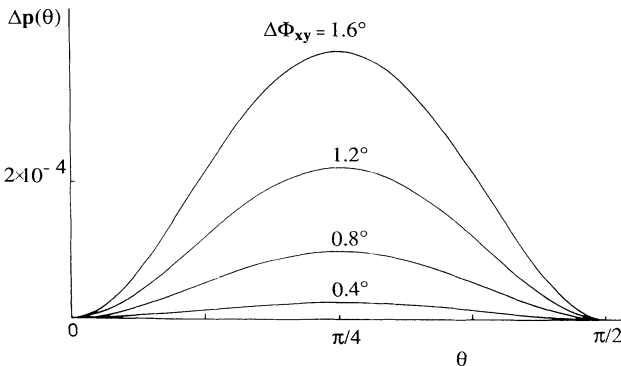


FIG. 2. Losses $\Delta p(\theta)$ of the amplitude of the field E after one round trip, vs the rotation angle θ , for different anisotropy values.

increase the laser frequency from the threshold. As stated above, the laser oscillates initially on the x eigenstate. Then for $\nu = \nu_0$, the working point is in the well A as shown in Fig. 3(a). We note the existence of a second well B corresponding to the nonoscillating y eigenstate. The two wells A and B are separated by a potential barrier due to the rotation losses $\Delta p(\theta)$. If the relative heights of A and B are varied by increasing the laser frequency for instance, the polarization can rotate from x to y and for $\nu_x = \nu_0 + 50$ MHz [Fig. 3(b)], it is the y eigenstate which now oscillates. The existence of these two potential wells A and B related to the two different order parameters E_x and E_y implies that the rotation of the polarization corresponds to a first-order phase transition and so occurs with hysteresis when the laser frequency is scanned. As the rotation losses vary like $\Delta\Phi_{xy}^2$, for greater anisotropy values the barrier becomes so high that we can expect that the rotation mechanism no longer occurs.

For greater anisotropy values, i.e., $\Delta\Phi_{xy} \gtrsim 1.3^\circ$ as it will be confirmed experimentally, the differences between the resonance frequencies are too large and the oscillators E_x and E_y are no longer locked together. So during the flip two oscillators oscillate simultaneously at frequencies ν_x and ν_y , respectively. The time behavior of the eigenstates amplitudes can be written in a form derived from Lamb's theory [4,7,8],

$$\dot{E}_x = E_x (\alpha_x - \beta_x E_x^2 - \theta_{xy} E_y^2), \quad (7)$$

$$\dot{E}_y = E_y (\alpha_y - \beta_y E_y^2 - \theta_{yx} E_x^2), \quad (8)$$

where α_x and α_y are the net gain coefficients and β_x, β_y and θ_{xy}, θ_{yx} the self- and cross-saturation coefficients. The steady-state solution for the amplitude of the two competing eigenstates can be associated, as in a laser with two longitudinal modes [30], with a potential

$$V(E_x, E_y) = -\frac{1}{2}\alpha_x E_x^2 - \frac{1}{2}\alpha_y E_y^2 + \frac{1}{4}\beta_x E_x^4 + \frac{1}{4}\beta_y E_y^4 + \frac{1}{2}\theta_{xy} E_x^2 E_y^2, \quad (9)$$

where we have assumed that $\theta_{xy} = \theta_{yx}$. The potential $V(E_x, E_y)$ and the corresponding equipotential curves are represented in Figs. 4(a) and 4(b) for $\nu_x = \nu_0$ and $\nu_x = \nu_0 + 50$ MHz, respectively. The barrier between the two wells A and B corresponding to the x and y eigenstates, respectively, is due in this case to a strong-coupling value $C = \theta_{xy} \theta_{yx} / \beta_x \beta_y > 1$. The variations of the relative heights of A and B obtained by scanning the laser frequency lead to a mode inhibition. During the x -to- y flip for instance, the x eigenstate oscillating at frequency ν_x switches off while simultaneously the y eigenstate switches on at a different frequency ν_y . The existence of this barrier related to two order parameters implies that the inhibition mechanism corresponds also to a first-order phase transition and occurs with hysteresis.

So, the spatial representation of the generalized potentials associated with the two linear eigenstates of a quasi-isotropic laser, in the frame of the Landau theory, predicts two different types of first-order phase transitions with corresponding polarization flips and hysteresis loops [31]. Their nature being quite different, we analyze sepa-

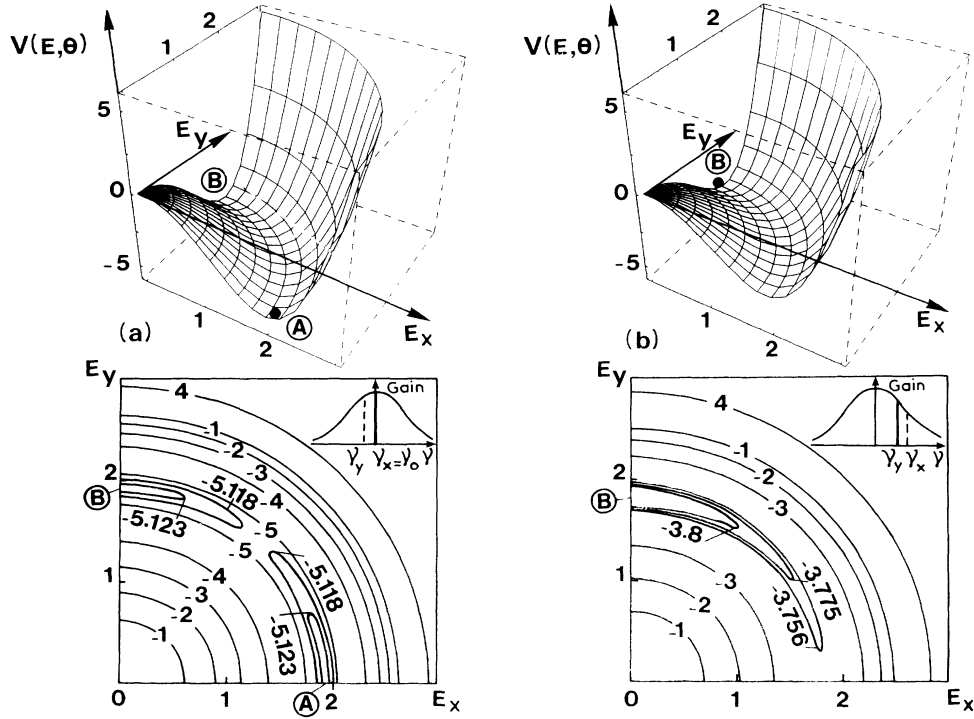


FIG. 3. Deformation of the potential $V(E, \theta)$ following the position of the eigenstates frequencies within the Doppler profile for $\Delta\Phi_{xy} = 1.2^\circ$. $\alpha_0 = 139 \times 10^6 \text{ s}^{-1}$; $\beta_0 = 13.9 \times 10^6 \text{ s}^{-1}$; $p = 83 \times 10^6 \text{ s}^{-1}$; $L = 0.54 \text{ m}$; $\Delta\nu_D = 350 \text{ MHz}$; $\gamma = 60 \text{ MHz}$. The potential unit is 10^7 s^{-1} . (a) $\nu_x = \nu_0$ (ν_0 is the resonance frequency of the atomic transition). *Top*: spatial representation of $V(E, \theta)$; *bottom*: corresponding equipotential curves. (b) $\nu_x = \nu_0 + 50 \text{ MHz}$. *Top and bottom*: same as in (a). Note that there is no stable solution any more on the x axis.

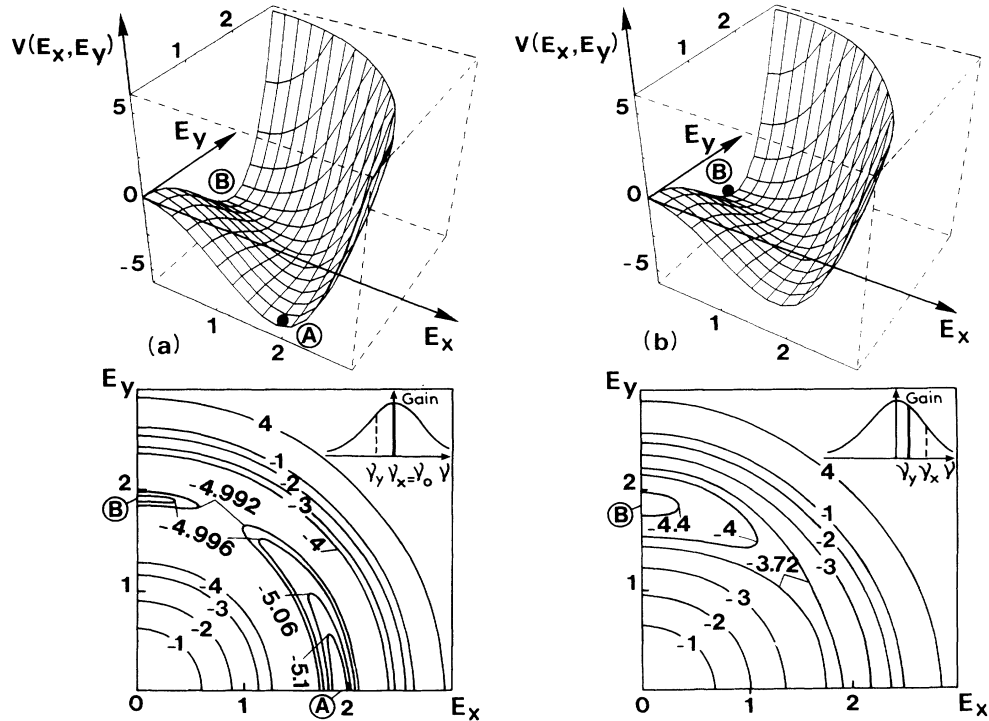


FIG. 4. Deformation of the potential $V(E_x, E_y)$ following the position of the eigenstates frequencies within the Doppler profile for $\Delta\Phi_{xy} = 10^\circ$. The potential unit is 10^7 s^{-1} . (a) $\nu_x = \nu_0$. *Top*: spatial representation of $V(E_x, E_y)$; *bottom*: corresponding equipotential curves. $\alpha_x = 56 \times 10^6 \text{ s}^{-1}$; $\alpha_y = 55.98 \times 10^6 \text{ s}^{-1}$; $\beta_x = 15.290 \times 10^6 \text{ s}^{-1}$; $\beta_y = 15.287 \times 10^6 \text{ s}^{-1}$; $\theta_{xy} = 15.5 \times 10^6 \text{ s}^{-1}$. (b) $\nu_x = \nu_0 + 50 \text{ MHz}$. *Top and bottom*: same as in (a). Note that there is no stable solution any more on the x axis. $\alpha_x = 45.10 \times 10^6 \text{ s}^{-1}$; $\alpha_y = 50.68 \times 10^6 \text{ s}^{-1}$; $\beta_x = 13.56 \times 10^6 \text{ s}^{-1}$; $\beta_y = 14.37 \times 10^6 \text{ s}^{-1}$; $\theta_{xy} = 15.5 \times 10^6 \text{ s}^{-1}$.

rately in the following sections the flip of the polarization in these two mechanisms, when the laser frequency is scanned, for instance, so as to compare with the experimental results.

B. The rotation mechanism

1. The flip condition

As the polarization does not remain strictly linear during the rotation, due to the phase anisotropy, the model introduced in the preceding paragraph for the prediction of the rotation mechanism must be completed for a quantitative study of this process. The ellipticity of the polarization induces in the active medium a circular phase anisotropy. Indeed, any elliptically polarized field is the sum of two circularly polarized components with different amplitudes E_+ and E_- and the corresponding saturated indexes are different. So the variation of the phase between the circular components leads to the rotation of the main polarization axis. The evolution of the polarization can be derived, as done by Tomlinson and Fork [11], from the differential equations which describe the time behavior of the amplitudes E_+ and E_- and of their corresponding phases Φ_+ and Φ_- . As pointed out by de Lang and van Haeringen [9,10] the polarization state can also be expressed in terms of the orientation θ of the main axis, of the ellipticity

$$\chi = \tan^{-1}(E_- - E_+) / (E_- + E_+)$$

and of the total intensity $I = E_+^2 + E_-^2$ of the elliptically polarized field. In Appendix B, expressions for θ and χ are given by calculating separately three contributions, i.e., that of the active medium and that of the phase and loss anisotropies. In particular, the role of these anisotropies on an incident elliptically polarized field is derived directly. By adding all contributions we get finally the same results as in [10] which are obtained by introducing in the electromagnetic field wave equation a loss tensor containing the isotropic cavity loss as well as the initial cavity anisotropies. For comparison with experimental results, in Appendix C an approximated analytic condition for the polarization flip including all anisotropies is derived from these equations. Without any x - y loss anisotropy, the flip condition from the x to the y eigenstate, for instance, can be derived from Eq. (C5) and is written as

$$\left[-\frac{1}{2} \frac{\rho_+}{\beta_+} \Delta\Phi_{xy} \right] + \left[\frac{c}{L} \frac{1}{4\alpha_+} \frac{S+1}{2S} \Delta\Phi_{xy}^2 \right] > 0. \quad (10)$$

The first term in square brackets represents the effect of the medium. The ratio ρ_+/β_+ of the dispersive and absorptive nonlinear coefficients versus the frequency may be written [10] as

$$\rho_+/\beta_+ = \frac{(\nu_0 - \nu)/\gamma}{2 + [(\nu_0 - \nu)/\gamma]^2} + 8[(\nu_0 - \nu)/\Delta\nu_D](\gamma/\Delta\nu_D). \quad (11)$$

The second term of Eq. (10) represents the effect of the linear phase anisotropy. It depends not only on $\Delta\Phi_{xy}$ but

also on the medium which acts on the ellipticity of the polarization [see Appendix C, Eq. (C2)]. $S = -\frac{3}{20}$ for a $J=1 \rightarrow J=2$ transition and α_+ is the net gain of the σ^+ component and is defined by

$$\alpha_+ = \alpha_0 \exp \left[- \left[\frac{\nu - \nu_0}{\Delta\nu_D/2} \right]^2 \right] - p. \quad (12)$$

The effects of the active medium and of the anisotropy can be in competition according to the frequency offset from ν_0 . Indeed, the medium leads to the rotation from x to y for $\nu > \nu_0$ as the ratio $-\rho_+/\beta_+$ is positive while the anisotropy defavors this rotation as S is negative. If the effect of the medium can overcome the effect of the anisotropy the polarization flips following the rotation mechanism [32]. For a more convenient graphical resolution, so as to compare with experimental results, the flipping conditions are written as

$$\frac{2\alpha_+ L}{c} \left[\frac{2S}{S+1} \right] \left[\pm \frac{\rho_+}{\beta_+} \right] \Delta\Phi_{xy} > \Delta\Phi_{xy}^2, \quad (13)$$

where $+$ and $-$ signs correspond to the x -to- y and y -to- x flips, respectively.

2. Evolution of the hysteresis loop with the anisotropy. Comparison with experiment

The solid and dashed lines in Figs. 5(a) and 5(b) represent, respectively, the left- and right-hand sides of the x -to- y and y -to- x flip conditions (13) versus the frequency for different phase-anisotropy values. The α_0 value which appears in the α_+ term is deduced from the average losses per second p which are known and from the experimental oscillation range. We shall use the results of a third-order theory even for pump parameter values higher than the usual limit value ($\eta \approx 1.2$). Indeed, the third-order theory results are found to be quite close to those given by a high-intensity theory for the 3.39- μm line considered [33]. The theoretical hysteresis loops are shown in Fig. 5(c). For a very small anisotropy value the active medium overcomes the effect of the anisotropy for a frequency near ν_0 allowing the flip. When the anisotropy increases the width of the hysteresis loop also increases. Indeed, according to Eq. (10) the effect of the medium varies linearly with $\Delta\Phi_{xy}$ while the effect of the anisotropy varies as $\Delta\Phi_{xy}^2$. So when the anisotropy increases the polarization can flip only at a frequency farther from ν_0 for which the effect of the medium is greater. We can note also the existence of a maximum anisotropy value ($\Delta\Phi_{xy} \approx 1.3^\circ$) for which the effect of the medium can be just sufficient to compensate the effect of the anisotropy. In this case the hysteresis loop is the greatest. Note that this maximum anisotropy value depends on the laser excitation as can be deduced from the study of the evolution of the hysteresis loop with the excitation done in the next section. For greater anisotropy values, for instance, $\Delta\Phi_{xy} = 1.5^\circ$, the medium cannot overcome the effect of the anisotropy and the rotation mechanism no longer occurs.

Experimental study of the two processes and of their

properties is performed with a 3.39- μm external cavity laser. The discharge tube, magnetically shielded, has a 5 mm inner diameter and is filled with a 7:1 ^3He - ^{20}Ne gas mixture at a total pressure of about 1 Torr. It is closed with slightly tilted windows in order to avoid any spurious Fabry-Pérot effects. The cavity is composed by two mirrors with a radius of curvature of 1.2 m. The output mirror reflectivity is 64% while the other one's is 95%. The cavity length in this experiment is $L = 54$ cm. The laser oscillates on a single longitudinal mode and a diffracting aperture selects only the TEM_{00} fundamental Gaussian mode. The adjustable linear birefringence $\Delta\Phi_{xy}$ can be measured outside the cavity as function of the stress F_x . A polarizer aligned along one of the birefringence axes in front of the output mirror allows us to investigate the hysteresis domain and also to detect the rotation mechanism if peaks or dips appear when the po-

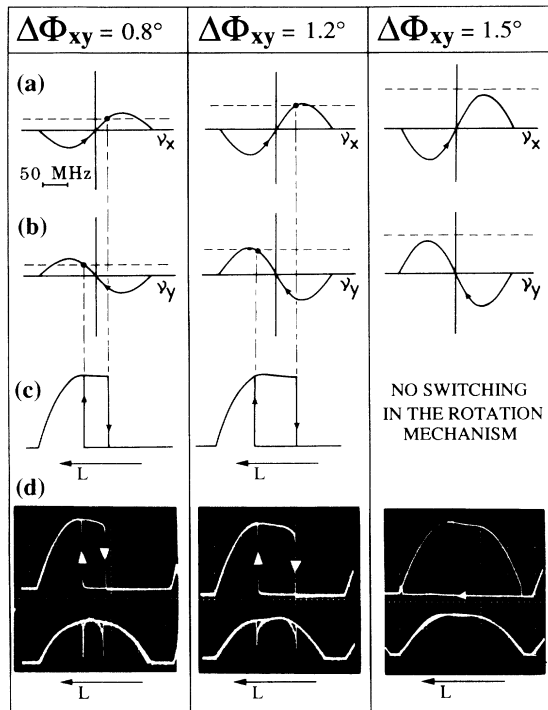


FIG. 5. Theoretical and experimental increase of the hysteresis loop with the phase anisotropy $\Delta\Phi_{xy}$ in the rotation mechanism. (a) Graphical resolution of the x -to- y flip condition (13). The arrows represent the frequency sweep direction. (b) Graphical resolution of the y -to- x flip condition. (c) Theoretical hysteresis loops. $\alpha_0 = 128 \times 10^6 \text{ s}^{-1}$; $p = 83 \times 10^6 \text{ s}^{-1}$ (the corresponding pump parameter is $\eta = 1.5$). (d) Experimental hysteresis loops. *Top*: the polarizer in front of the detector is along the x axis. The intensity on the x axis is I_x (I_x axis, $3\mu\text{W}/\text{div}$; L axis, $60 \text{ MHz}/\text{div}$). *Bottom*: the polarizer in front of the detector is at 45° from the x axis. The dips show that the polarization flips following the rotating mechanism. Note that in (a) and (b) the horizontal axes represent the frequencies ν_x and ν_y , respectively, while in (c) and (d) the axes represent the experimental parameter, i.e., the cavity length L . The shift between the origins of the ν_x and ν_y frequency axes is proportional to $\Delta\Phi_{xy}$ and is here negligible.

larizer is rotated at $\pm 45^\circ$ from the x axis. The experimental evolution of the hysteresis loop with the anisotropy is reported in Fig. 5(d) (top curves). In Fig. 5(d) (bottom curves) the rotation dips appear distinctly. We can note that for an increase of the laser frequency, i.e., for a decrease of the cavity length L obtained by a piezoelectric transducer, the oscillation always starts on the x axis because the x eigenstate is the first above the threshold. The experimental hysteresis loops [Fig. 5(d)] are found to be in good agreement with the theoretical ones [Fig. 5(c)].

3. Evolution of the hysteresis loop with the excitation. Comparison with experiment

Contrary to the preceding analysis, here the anisotropy is fixed at $\Delta\Phi_{xy} = 1.2^\circ$ and the laser excitation varies, the other experimental parameters remaining unchanged. The x -to- y and y -to- x flip conditions are represented, respectively, in Figs. 6(a) and 6(b) for three values of the laser excitation current. The corresponding theoretical hysteresis loops in Fig. 6(c) show that the width of the hysteresis loop increases when the excitation decreases. Indeed, when the excitation decreases the effect of the anisotropy [second term of (10)] increases so that the medium can overcome the effect of the anisotropy only for a frequency farther from ν_0 . This theoretical evolution of the hysteresis loop is verified experimentally in Fig. 6(d) (top curves). In Fig. 6(d) (bottom curves), the rotation dips are visible for high excitation values. For a low current value about 8 mA we verify that the rotation dips

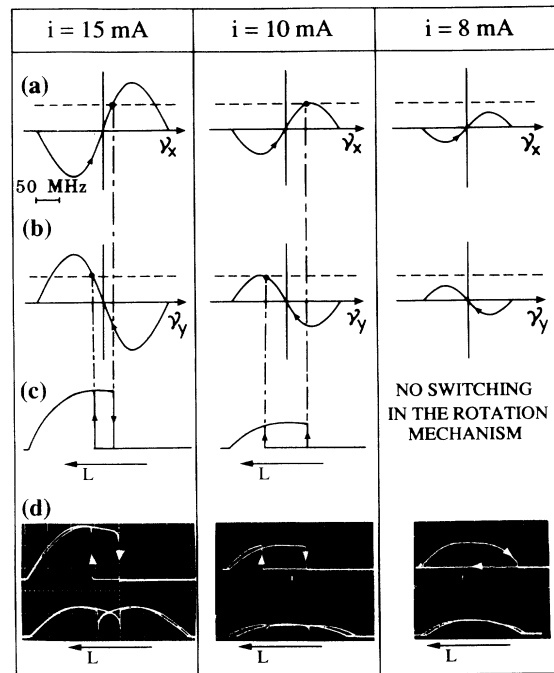


FIG. 6. Theoretical and experimental increase of the hysteresis loop when the current decreases in the rotation mechanism: (a)–(d) same as in Fig. 5. L axis: $50 \text{ MHz}/\text{div}$; $\alpha_0 = 158 \times 10^6 \text{ s}^{-1}$ for $i = 15 \text{ mA}$; $\alpha_0 = 128 \times 10^6 \text{ s}^{-1}$ for $i = 10 \text{ mA}$; $\alpha_0 = 111 \times 10^6 \text{ s}^{-1}$ for $i = 8 \text{ mA}$; $p = 83 \times 10^6 \text{ s}^{-1}$.

disappear. The system switches then in the inhibition mechanism which we are now going to investigate.

C. The inhibition mechanism

1. The flip condition

As stated above, the system switching following the inhibition mechanism may be considered during the flip as two independent oscillators which oscillate at two different frequencies. Following Lamb's analysis [4] used for a laser with two longitudinal modes with the same linear polarization, the condition for the flip from x to y is written

$$\alpha_y - \theta_{yx} I_x > 0, \quad (14)$$

where $I_x = \alpha_x / \beta_x$ is the intensity of the x oscillating eigenstate. This condition means that the y eigenstate builds up if its net gain α_y is sufficiently large to overcome the competition term $\theta_{yx} I_x$. In other words, this last term represents the self-stabilization of the x lasing eigenstate to resist the onset of the y eigenstate. In a similar way the y -to- x flip condition is

$$\alpha_x - \theta_{xy} I_y > 0, \quad (15)$$

with $I_y = \alpha_y / \beta_y$. The different coefficients appearing in the flip conditions (14) and (15) have been calculated in [8]. Their frequency variations are similar to those obtained by Lamb in the scalar case [4]. Let us recall below these expressions in the absence of velocity-changing collisions [34–36]. The net gain α_i ($i = x, y$) is written as

$$\alpha_i = \alpha_0 \exp \left[- \left[\frac{\nu_i - \nu_0}{\Delta \nu_D / 2} \right]^2 \right] - p_i, \quad (16)$$

where p_i represents the average losses per second of the eigenstate i . The self-saturation β_i is

$$\beta_i = \beta_0 [1 + L(\nu_0 - \nu_i)] \exp \left[- \left[\frac{\nu_i - \nu_0}{\Delta \nu_D / 2} \right]^2 \right], \quad (17)$$

where β_0 depends on the atomic parameters and on the excitation. The Lorentzian L is defined by

$$L(\nu_0 - \nu_i) = \gamma^2 / [\gamma^2 + (\nu_0 - \nu_i)^2].$$

The cross-saturation coefficient θ_{ij} can be written if we neglect spatial hole burning effects [4],

$$\theta_{ij} = \theta_0 [L(\Delta \nu_{xy} / 2) + L(\nu_0 - \nu_i / 2 - \nu_j / 2)] \times \exp \left[- \left[\frac{\nu_i - \nu_0}{\Delta \nu_D / 2} \right]^2 \right]. \quad (18)$$

For $\Delta \nu_{xy} \ll 2\gamma$, i.e., for small birefringence values the expression of θ_{ij} reduces to

$$\theta_{ij} \approx \theta_0 [1 + L(\nu_0 - \nu_i)] \exp \left[- \left[\frac{\nu_i - \nu_0}{\Delta \nu_D / 2} \right]^2 \right], \quad (19)$$

so that an inhibition term such as $\theta_{yx} I_x$ becomes using (17) and (19)

$$\theta_{yx} I_x = (\theta_0 / \beta_0) \alpha_x. \quad (20)$$

The coupling constant can be written as

$$C = \theta_{xy} \theta_{yx} / \beta_x \beta_y \approx (\theta_0 / \beta_0)^2$$

and the preceding inequalities (14) and (15) lead then to the following approximated x -to- y and y -to- x flip conditions:

$$\alpha_{y,x} - \sqrt{C} \alpha_{x,y} > 0. \quad (21)$$

As the coupling constant C between the two eigenstates is strong [37], that is $C > 1$, this implies vectorial bistability. Expressions (21) can still be used if we take into account the velocity-changing collisions and are sufficient to interpret the main properties of the inhibition mechanism.

2. Evolution of the hysteresis loop with the anisotropy. Comparison with experiment

We suppose here that the laser excitation is constant and that the losses p_x and p_y of the two eigenstates are equal (same value as in Fig. 5). As the gain and the inhibition terms of Eq. (21) are frequency shifted one from another proportionally to the anisotropy value, the flip conditions will be fulfilled at different crossing points of the corresponding curves. So for a small anisotropy

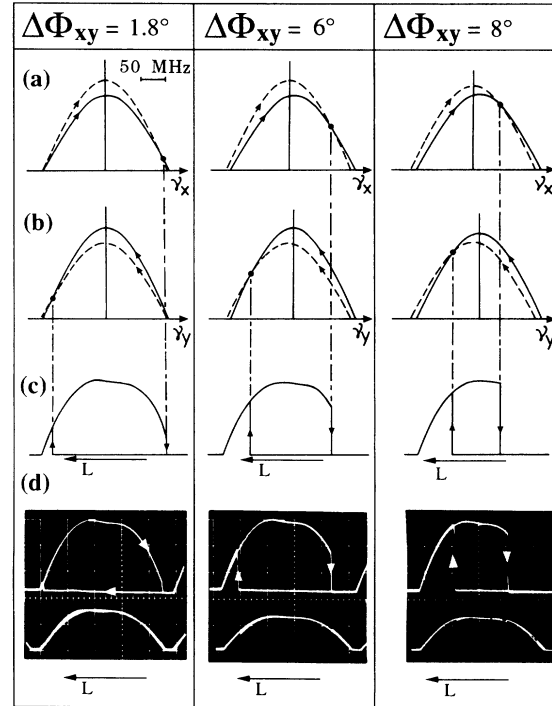


FIG. 7. Theoretical and experimental decrease of the hysteresis loop when the phase anisotropy $\Delta \Phi_{xy}$ increases in the inhibition mechanism. (a) Representation of the x -to- y flip condition. (b) Representation of the y -to- x flip condition. (c),(d) Theoretical and experimental hysteresis loops (I_x axis, $3\mu\text{W/div}$; L axis, 60 MHz/div). Note that for large values of $\Delta \Phi_{xy}$ the shift between the origins of the ν_x and ν_y frequency axes is noticeable. $\alpha_0 = 139 \times 10^6 \text{ s}^{-1}$; $C = 1.4$ for low anisotropy and 1.2 for 8° .

value Eq. (21) will be satisfied near threshold and as the anisotropy increases at a frequency value nearer the frequency ν_0 . This evolution is confirmed in Fig. 7 for increasing values of $\Delta\Phi_{xy}$. In Fig. 7(a) the solid and the dashed lines represent the α_y and the $\theta_{yx}I_x \approx \sqrt{C}\alpha_x$ terms, respectively. The reverse y -to- x flip condition is represented in Fig. 7(b), where the dashed lines represent the α_x term while the solid lines represent the $\theta_{xy}I_y \approx \sqrt{C}\alpha_y$ term. The corresponding hysteresis loops are represented in Fig. 7(c). For $\Delta\Phi_{xy} = 1.8^\circ$ the inhibition mechanism appears at a low-intensity value near threshold. The hysteresis domain then occupies almost the whole laser intensity profile. When the anisotropy increases the net gain of the nonoscillating eigenstate can compensate the inhibition term only for a frequency nearer the resonance frequency of the atomic transition ν_0 . So in contrast to the rotation mechanism, in the inhibition mechanism the hysteresis loop shrinks for increased values of $\Delta\Phi_{xy}$. The experimental hysteresis loops in Fig. 7(d) (top curves) obtained with the setup used above for the rotation mechanism are in good agreement with the theoretical curves. In Fig. 7(d) (bottom curves), the absence of peaks or dips with the polarizer at $+45^\circ$ from the x axis confirms that the flips occur in the inhibition mechanism.

3. Evolution of the hysteresis loop with the excitation. Comparison with experiment

According to the flip condition (21) we can note that an increase of the intensity of the oscillating mode stabilizes this mode more and leads then to an increase of the hysteresis loop width. This can be verified by representing the x -to- y and y -to- x flip conditions (21) in Figs. 8(a) and 8(b), respectively, for different laser excitation values. In this experiment the anisotropy is constant and fixed at $\Delta\Phi_{xy} = 4^\circ$ and the length of the cavity is now $L = 44$ cm. The hysteresis loops in Fig. 8(c) show that the hysteresis domain shrinks here when the current decreases as shown by the corresponding experimental curves in Fig. 8(d) (top curves). The absence of peaks or dips in Fig. 8(d) (bottom curves) shows that the polarization switches again following the inhibition mechanism.

4. Peculiar evolutions of the hysteresis loop

Until now we have studied the evolution of the hysteresis loop with the anisotropy and with the excitation for birefringence values such as $\Delta\nu_{xy} \ll 2\gamma$. We investigate here what happens in lasers when this condition is no longer satisfied, i.e., for high anisotropy values and for low gas pressure which leads to a low γ value. In this case the approximation $\theta_{yx}I_x \approx \sqrt{C}\alpha_x$ is no longer valid. With use of expressions (17) and (18), the inhibition term is then written as

$$\theta_{yx}I_x = \frac{\theta_0 L (\Delta\nu_{xy}/2) + L (\nu_0 - \nu_x/2 - \nu_y/2)}{\beta_0 (1 + L (\nu_0 - \nu_x))} \alpha_x. \quad (22)$$

As resonances appear in this inhibition term we can expect peculiar evolutions of the hysteresis loop.

Let us first consider the evolution of the hysteresis loop

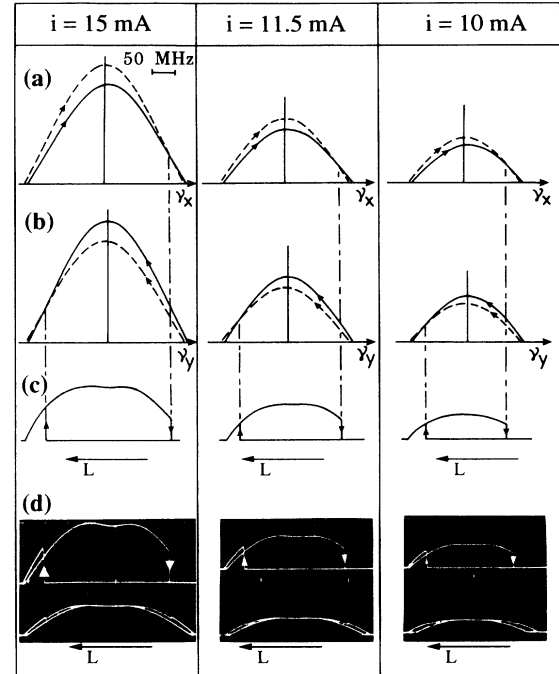


FIG. 8. Theoretical and experimental decrease of the hysteresis loop with the excitation current in the inhibition mechanism. (a)–(d) same as in Fig. 7. L axis: 50 MHz/div; $C = 1.4$; $\alpha_0 = 262 \times 10^6 \text{ s}^{-1}$ for $i = 15$ mA; $\alpha_0 = 188 \times 10^6 \text{ s}^{-1}$ for $i = 11.5$ mA; $\alpha_0 = 163 \times 10^6 \text{ s}^{-1}$ for $i = 10$ mA; $p_x = p_y = 102 \times 10^6 \text{ s}^{-1}$.

with the anisotropy $\Delta\Phi_{xy}$ in the case where different losses between the x and y eigenstates are introduced. This will be obtained by tilting the stressed plate for instance [38]. In Fig. 9 we have displayed with the same graphical representations used previously the two flipping conditions (21) with $p_x > p_y$ for two different values of $\Delta\Phi_{xy}$. For the x -to- y flip [Fig. 9(a)] we find when the anisotropy value is increased from 10° to 12° a new crossing point between the two curves below the atomic transition frequency ν_0 . On the contrary, for the y -to- x flip [Fig. 9(b)] there is practically no change for the crossing point. So, the width of the hysteresis loop abruptly shrinks as shown in Fig. 9(c) when the anisotropy is slightly increased. The whole bistable domain is below ν_0 corresponding to a smaller frequency domain for the x eigenstate oscillation. The corresponding experimental evolution shown in Fig. 10 for $p_x > p_y$ is in agreement with this analysis. On the contrary, if we choose $p_y > p_x$ we obtain a similar evolution but now with the whole bistable domain above ν_0 . We can notice that this peculiar evolution occurs only for low gas pressure of about 0.8 Torr. Indeed, for higher gas pressure (≈ 1.4 Torr) the Lamb dip disappears and we observe then a continuous shrink of the hysteresis loop when the anisotropy is increased (Fig. 11).

Let us now consider another possibility for having new crossing points at a lower gas pressure (≈ 0.6 Torr). Taking account of the expression (22) for the inhibition

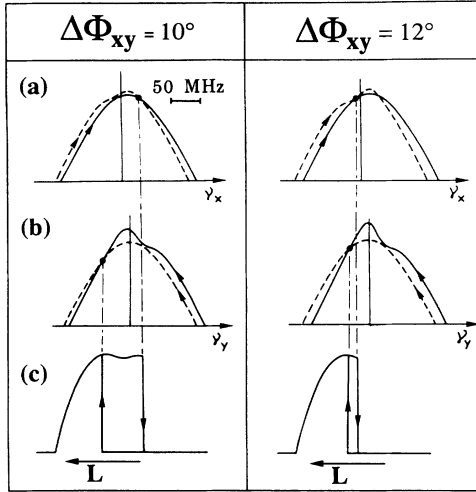


FIG. 9. Theoretical evolution of the hysteresis loop with the phase anisotropy ($\Delta\Phi_{xy} \geq 10^\circ$) in the inhibition mechanism for low gas pressure (≈ 0.8 Torr). (a),(b) Representation of the x -to- y and y -to- x flip conditions, respectively. (c) Corresponding hysteresis loops. Note the abrupt shrink of the bistable domain for $\Delta\Phi_{xy} = 12^\circ$; $p_x - p_y = 1.6 \times 10^6 \text{ s}^{-1}$.

term the x -to- y and y -to- x flip conditions represented in Fig. 12 show that new crossing points appear when the laser excitation increases. So, the x -to- y and y -to- x flips can occur at several frequencies. There are *multiple switchings* when the laser frequency increases as shown in Fig. 12(c) due to the enhancement of the Lamb dip appearing in the inhibition term $\theta_{yx} I_x$ at low gas pressure.

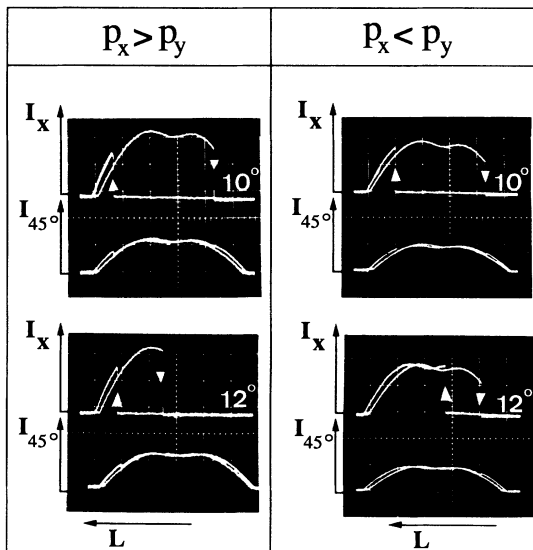


FIG. 10. Experimental evolution of the hysteresis loop with the phase anisotropy in the inhibition mechanism for low gas pressure (≈ 0.8 Torr). $p_x > p_y$. Top: $\Delta\Phi_{xy} = 10^\circ$. Bottom: $\Delta\Phi_{xy} = 12^\circ$. The hysteresis loop evolution is in agreement with the corresponding theoretical one [Fig. 9(c)]. $p_x < p_y$. Top: $\Delta\Phi_{xy} = 10^\circ$. Bottom: $\Delta\Phi_{xy} = 12^\circ$.

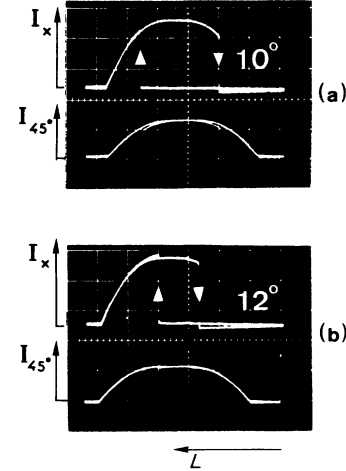


FIG. 11. Experimental evolution of the hysteresis loop with the phase anisotropy in the inhibition mechanism for high gas pressure (≈ 1.4 Torr). The hysteresis domain shrinks continuously. (a) $\Delta\Phi_{xy} = 10^\circ$. (b) $\Delta\Phi_{xy} = 12^\circ$.

This new behavior is also well verified by the experimental curves in Fig 13.

In preceding sections we have considered hysteresis loops for which the switchings occur in the same process, i.e., either in the rotation or in the inhibition mechanism. A last question then arises: Is it possible to obtain one of each mechanism for a given hysteresis loop, i.e., to realize finally a *hybrid* hysteresis loop?

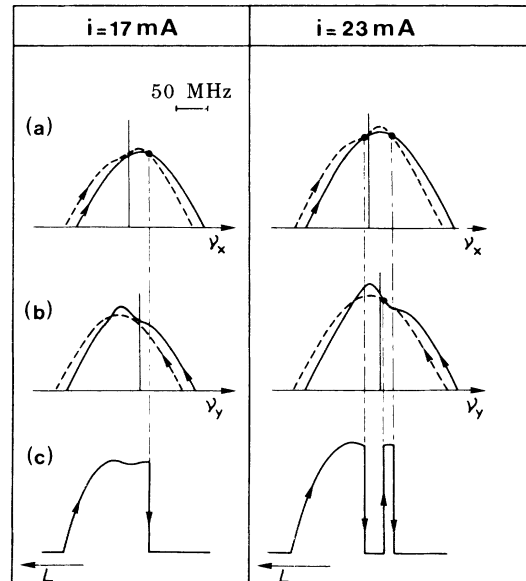


FIG. 12. Theoretical evolution of the polarization switching with the current in the inhibition mechanism for low gas pressure (≈ 0.6 Torr). $\Delta\Phi_{xy} = 12^\circ$. (a),(b) Representation of the x -to- y and y -to- x flip conditions, respectively. (c) Corresponding switchings when the laser frequency increases. For an increase of the current value, multiple switchings appear.

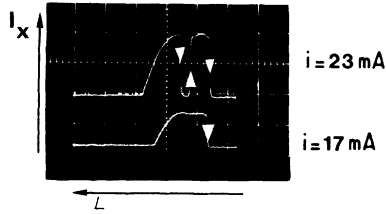


FIG. 13. Experimental results corresponding to the theoretical Fig. 12(c) for low gas pressure (≈ 0.6 Torr).

D. Hybrid hysteresis loop

Realization of any hybrid hysteresis loop needs, on the one hand, to choose the phase anisotropy near the frontier value of the two mechanisms. On the other hand, to allow the rotation only in one direction during the scan prohibiting it in the other direction, one must favor one eigenstate by decreasing its losses. This can be obtained, for instance, by tilting an internal plate. Taking into account the x - y -type loss anisotropy introduced by the tilted plate, the flip condition from x to y derived in Appendix C [Eq. (C5)] may be written as

$$\frac{2\alpha_+ L}{c} \left[\frac{2S}{S+1} \right] \left[\frac{\rho_+}{\beta_+} \Delta\Phi_{xy} - (t_y/t_x - 1) \right] > \Delta\Phi_{xy}^2, \quad (23)$$

where t_x and t_y are the transmission coefficients of the tilted plate for the field amplitude and where we have assumed that $t_y/t_x \approx 1$. In a similar way the y -to- x flip condition is obtained by changing the sign of the two terms in square brackets.

We have represented the two flipping conditions in Figs. 14(a) and 14(b), respectively. The phase anisotropy is fixed at the maximum limit value for the rotation process, i.e., $\Delta\Phi_{xy} = 1.7^\circ$ for the excitation current considered here and the y eigenstate is favored, i.e., $t_y > t_x$ with $t_y/t_x - 1 = 2 \times 10^{-3}$. Figure 14(a) shows that the effect of the loss anisotropy favors the rotation from x to y when the frequency increases. On the contrary, when the frequency decreases the losses no longer favor this process and the effect of the medium is not sufficient to produce the rotation. Then the system switches following the inhibition mechanism as shown in Fig. 14(c) where the y -to- x flip condition (21) is represented. For the small value of the phase anisotropy considered here this switching occurs at a frequency near the threshold. This leads to the theoretical hybrid hysteresis loop represented in Fig. 14(d) which corresponds to the experimental hysteresis loop reported in Fig. 15(a). If now the x eigenstate is favored the polarization switches then following the inhibition mechanism when the laser frequency increases and following the rotation mechanism when it decreases as shown in Fig. 15(b).

Until now we have investigated the properties of the basic polarization flipping mechanisms in gas lasers. One may wonder what processes appear in usual macroscopic and microscopic quasi-isotropic lasers that show polarization flips. We can also wonder if this vectorial bistability can be observed versus parameters other than the laser frequency. As an example let us consider a micro-

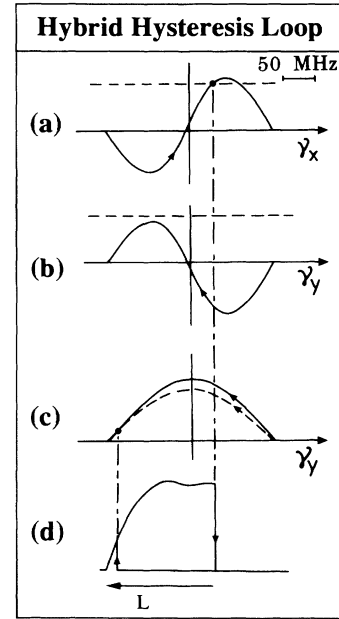


FIG. 14. Theoretical hybrid hysteresis loop. (a),(b) Representation of the switching conditions in the rotation mechanism when the laser frequency increases and decreases, respectively. (c) Representation of the y -to- x switching condition in the inhibition mechanism, when the laser frequency decreases. (d) Corresponding hybrid hysteresis loop. $\alpha_0 = 141 \times 10^6 \text{ s}^{-1}$; $p = 83 \times 10^6 \text{ s}^{-1}$; $C = 1.4$.

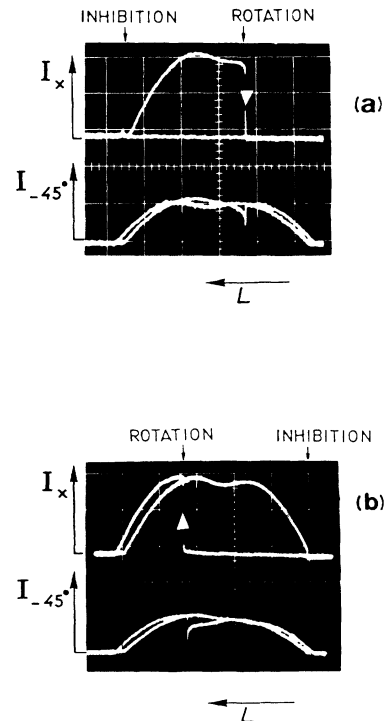


FIG. 15. Experimental hybrid hysteresis loop. (a) $p_x > p_y$. *Top*: hybrid bistable domain corresponding to Fig. 14(d). *Bottom*: polarizer at -45° from the x eigenstate allows to detect the two processes. (b) $p_x < p_y$. *Top*: hybrid bistable domain. *Bottom*: detection of the two mechanisms.

scopic system such as a TE-TM bistable semiconductor laser.

E. Polarization flip in bistable semiconductor lasers

In a semiconductor laser the possible eigenstates are polarized parallel (TE modes) and perpendicular (TM modes) to the junction. As the facet reflectivities are different for the TE and TM modes, for instance for an In-Ga-As-P/InP laser $R_{TE}=0.39$ and $R_{TM}=0.26$ [39], the oscillation occurs generally on the TE modes. However, it has been noticed that a stress can induce a greater gain for TM modes allowing their oscillation [39–41]. This stress can be obtained thermally, for instance, as done by Chen and Liu [41] by cooling In-Ga-As-P/InP lasers down to about 180 K. Taking into account the high phase-anisotropy values induced by the stress, we can predict that the polarization will flip following the inhibition mechanism. The condition for the flip from TM to TE modes is then similar to condition (21) derived above for a gas laser and is written [21] as

$$\alpha_{0E} - \theta_{EM}(P_E/P_M)\alpha_{0M} > 0, \quad (24)$$

where α_{0E} (α_{0M}) is the unsaturated net gain of TE (TM) mode, P_E (P_M) the losses of TE (TM) mode, and θ_{EM} the cross-saturation coefficient. In standard semiconductor lasers the frequency cannot be scanned as simply as in usual lasers. However, the current can be taken as the control parameter in this case. Indeed, as the increase of the α_{0E} gain versus current is greater than that of the α_{0M} gain [21] it will be possible, when condition (24) is fulfilled, to observe the TM-to-TE polarization flip with a current variation. Note that a variation of the current introduces also a small shift of the frequency which has no effect in the flipping mechanism as the width of the gain curve is quite large. Figure 16 displays the flips between TE and TM modes with hysteresis for a 1.3- μm semicon-

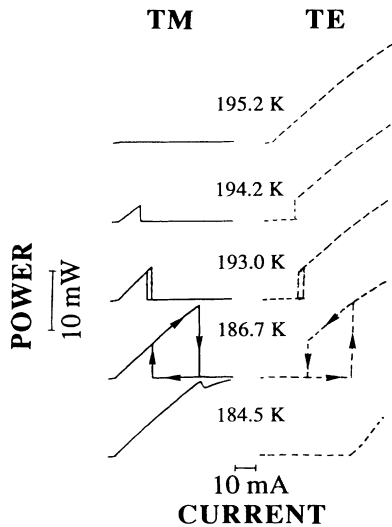


FIG. 16. Polarization-resolved power vs current characteristics of a polarization bistable laser at various temperatures (Ref. [20]).

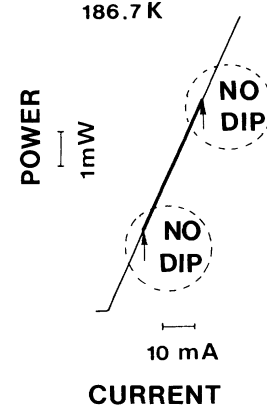


FIG. 17. Output power vs current with the polarizer at 45° from the TE direction: the absence of peaks or dips at the switching points (arrows) shows that the polarization flips following the inhibition mechanism.

ductor laser at low temperatures versus the injection current. If a polarizer is rotated at 45° from the eigenstates there is as shown in Fig. 17 no peak (nor dip) in the output power of the laser through the switching point confirming the inhibition process as predicted.

The inhibition mechanism may occur also in high-power CO_2 ring lasers [42]. Indeed, in this case for an odd number of mirrors, as each mirror is equivalent to a half-wave plate, the whole cavity is equivalent to a single half-wave plate leading to an important phase anisotropy $\Delta\Phi_{xy}$.

The knowledge of the eigenstates flipping processes and their corresponding properties in the laser itself when an internal parameter is varied allows us now to investigate the polarization control by an anisotropic feedback, i.e., in one-frequency systems.

III. CONTROL OF THE EIGENSTATES BY AN ANISOTROPIC FEEDBACK

The feedback method is usually performed to obtain single longitudinal mode operation [43], higher output power [44], and (or) frequency stability improvement [45]. As the feedback is isotropic in most of these devices, only scalar parameters such as, for instance, the intensity and the frequency can be changed. de Lang was the first to use an anisotropic feedback to modify the polarization to our knowledge [9]. More recently, Hendow *et al.* [16] experimentally controlled the polarization of an He-Ne laser with this method. Unfortunately, as the mirrors were sealed they could not control the anisotropy and the frequency, parameters which govern the two flipping processes. Let us try to isolate an induced-rotation and an induced-inhibition mechanism and interpret a polarization control in these two processes in a laser with an external cavity.

A. The principle of the control

The general setup for the polarization control is described in Fig. 18. The laser cavity with the mirrors M_1

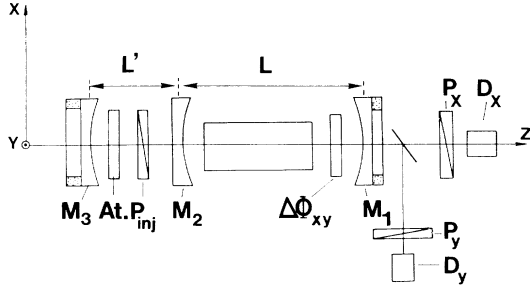


FIG. 18. General setup for the polarization control by an anisotropic feedback. P_x , P_{inj} are polarizers aligned along the x axis, P_y is along the y axis. At are additional calibrated attenuators and D_x , D_y are detectors.

and M_2 is coupled via the mirror M_2 to an anisotropic cavity composed by the mirrors M_2 and M_3 and by the polarizer P_{inj} . To prevent any modification of the x and y eigenstates directions the polarizer P_{inj} is aligned along the x axis. The anisotropic cavity is similar to an anisotropic mirror with equivalent mirror reflectivities R_{23}^x and R_{23}^y along the x and y axes, respectively. If we suppose that the laser oscillates on the y axis and that the polarizer in the feedback cavity is along the x axis then $R_{23}^y = R_2$. On the contrary, when the laser oscillates on the x axis the end mirror M_2 can be replaced by a Fabry-Pérot feedback cavity. For low feedback intensities the Fabry-Pérot reflectivity along the x axis is [46]

$$R_{23}^x = R_2 + 2a(R_2 R_3)^{1/2}(1 - R_2) \cos \Phi, \quad (25)$$

where a is the amplitude transmission of the attenuator for a round trip in the feedback cavity and $\Phi = 4\pi L' / \lambda$ is the phase of the return beam relative to the output beam, where L' is the feedback cavity length and λ is the laser wavelength. Expression (25) shows that R_{23}^x is maximum for $L' = m\lambda/2$ and is minimum for $L' = (2m + 1)\lambda/2$ where m is an integer. By varying the phase Φ the effective reflectivity R_{23}^x can be greater or smaller than R_{23}^y . So, the oscillation of the x eigenstate can be favored or not as seen later leading to a possible polarization control either in an induced-rotation or in an induced-inhibition process.

B. The induced-rotation mechanism

1. Shift of the hysteresis loop

We have seen that for the laser without feedback and with equal eigenstates losses, the hysteresis loop is symmetrical about ν_0 . According to Eq. (25) the anisotropic feedback cavity introduces a linear loss anisotropy which is written for a low transmission value

$$\left[\frac{R_{23}^y}{R_{23}^x} \right]^{1/2} \approx 1 - a \left[\frac{R_3}{R_2} \right]^{1/2} (1 - R_2) \cos \Phi. \quad (26)$$

With this feedback, as the x and y loss difference can be time modulated with $\Phi(t)$, we can predict a shift of the hysteresis loop. For example, the hysteresis loop will be

shifted towards high frequencies if the losses of the x eigenstate are lower than that of the y eigenstate. The x -to- y flip condition, for instance, can be obtained by letting $t_y/t_x = (R_{23}^y/R_{23}^x)^{1/2}$ in relation (23). Figure 19(a) shows the theoretical curves related to both sides of the relation (23) when the laser frequency is scanned for different Φ_0 values where Φ_0 is the feedback phase defined at $\nu = \nu_0$. Figure 19(b) gives the corresponding curves for the induced y to the x rotation. The resulting theoretical polarization hysteresis loops in Fig. 19(c) show that the hysteresis domain is indeed shifted with the phase Φ_0 while keeping a quasiconstant width. The experimental hysteresis loops shown in Fig. 19(d) are in good agreement with the theoretical curves. In this experiment the laser cavity length is $L = 48$ cm, the feedback cavity length is $L' = 57$ cm, the amplitude transmission of the attenuator is $a = 0.64$, and the phase anisotropy is $\Delta\Phi_{xy} = 1.3^\circ$. By varying the phase Φ_0 for a given laser cavity length we can then favor alternately the x and y eigenstate and so induce flips from x to y and y to x . We can hence realize optical gates.

2. Optical gates

Let us label L_a the maximum cavity length for the x -to- y flip and L_b the minimum cavity length for the y -to- x flip [Fig. 19(c)]. It will be possible to control the polar-

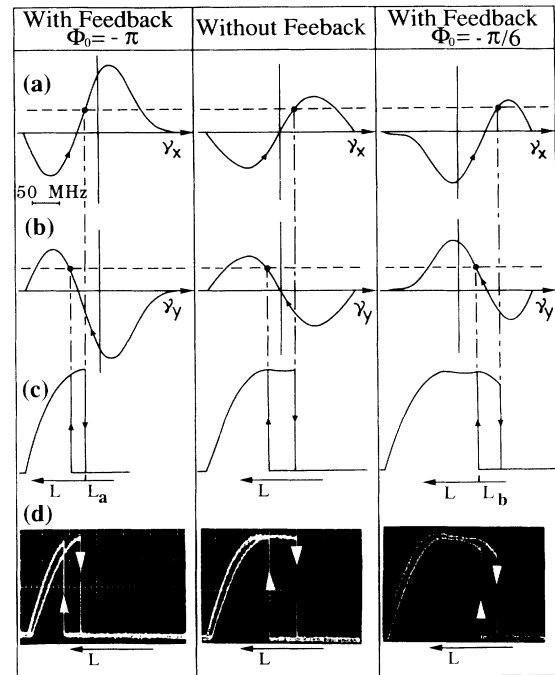


FIG. 19. Theoretical and experimental shifts of the hysteresis loop in the induced-rotation mechanism for two values of the external parameter Φ_0 . The unperturbed hysteresis loop is used as reference. (a),(b) Representation of the x -to- y and y -to- x flip conditions, respectively. $\alpha_0 = 168 \times 10^6 \text{ s}^{-1}$; $p = 94 \times 10^6 \text{ s}^{-1}$. (c),(d) Theoretical and experimental hysteresis loops. Output power I_x vs cavity length (I_x axis, $3\mu\text{W/div}$; L axis, 50 MHz/div).

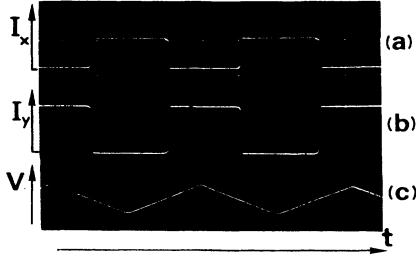


FIG. 20. Induced-rotation gate. (a) Output power I_x of the x eigenstate vs time (I_x axis, $10\mu\text{W}/\text{div}$; t axis, $10\text{ms}/\text{div}$). (b) Output power I_y of the y eigenstate vs time (I_y axis, $10\mu\text{W}/\text{div}$; t axis, $10\text{ms}/\text{div}$). (c) Sawtooth voltage applied to the feedback piezoelectric transducer (V axis, $50\text{V}/\text{div}$; t axis, $10\text{ms}/\text{div}$).

ization only if $L_a > L_b$ on the one hand, a condition which implies a shift of the hysteresis loop, and if the cavity length L is such as $L_a > L > L_b$ on the other hand. Then we obtain by modulating the feedback cavity length, i.e., Φ_0 , optical gates with high signal-to-noise ratios as show in Fig. 20. By rotating the polarizer P_y at -45° from the x eigenstate there are dips and peaks [Fig. 21(b)] in the transmitted intensity. The polarization control is then performed following the rotation mechanism. In contrast to the on-off logic (corresponding to high-low-level intensities) used in most scalar devices, this x - y polarization logic where the two orthogonal x and y eigenstates are the two logic states has several advantages. In particular, it seems well suited for cascading [47] where the remaining power on the off output of one gate can serve as input for the following gate. Furthermore, high sensitivity is expected in this polarization logic. We can evaluate the switching energy involved in the experiment by noting that for very weak return beams the feedback-induced power changes [46] are proportional to $2a(R_2R_3)^{1/2}(1-R_2)I$, where I is the internal laser intensity. For $a = 3.2 \times 10^{-4}$, $R_2 = R_3 = 0.64$, $I = 5\mu\text{W}$, and a typical switching time of $\tau = 1\mu\text{s}$, we obtain a switching energy of the order of 0.8fJ [48]. Femtojoule switching energy has also been obtained in scalar semiconductor laser amplifiers [49]. In this case the switching time is about 3ns , but the switching power is still of $1\mu\text{W}$.

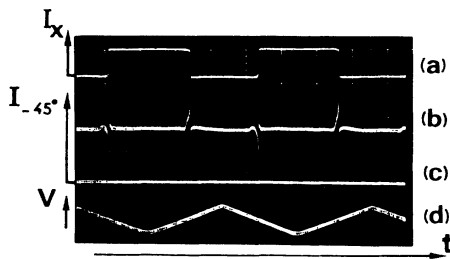


FIG. 21. Detection of the induced-rotation mechanism. (a) Same as in Fig. 21. (b) Output power with polarizer P_y at -45° from the x axis: induced-rotation dips and peaks are visible. (I_{-45° axis, $2.5\mu\text{W}/\text{div}$; t axis, $10\text{ms}/\text{div}$). (c) Zero intensity for I_{-45° . (d) Same sawtooth voltage as in Fig. 20.

For an anisotropy value greater than about 1.3° we have seen in Sec. II B 2 that, in the laser itself, the polarization does not flip any more following the rotation mechanism, but following the inhibition mechanism. In the next section we investigate the possibility of vectorial control in an induced-inhibition mechanism.

C. The induced-inhibition mechanism

1. The flip condition

The flip conditions are written here by taking into account the different losses p_x and p_y due to the anisotropic feedback. According to (25) these losses are written as

$$p_x = -\frac{1}{4} \frac{c}{L} \ln(R_1 R_2^3) \\ = -\frac{1}{4} \frac{c}{L} \ln(R_1 R_2) - \frac{c}{2L} a \left(\frac{R_3}{R_2} \right)^{1/2} (1-R_2) \cos\Phi, \quad (27a)$$

$$p_y = -\frac{1}{4} \frac{c}{L} \ln(R_1 R_2^3) = -\frac{1}{4} \frac{c}{L} \ln(R_1 R_2). \quad (27b)$$

The x -to- y and y -to- x flip conditions are represented in Figs. 22(a) and 22(b), respectively, when the laser frequency is scanned for different Φ_0 values. The anisotropy

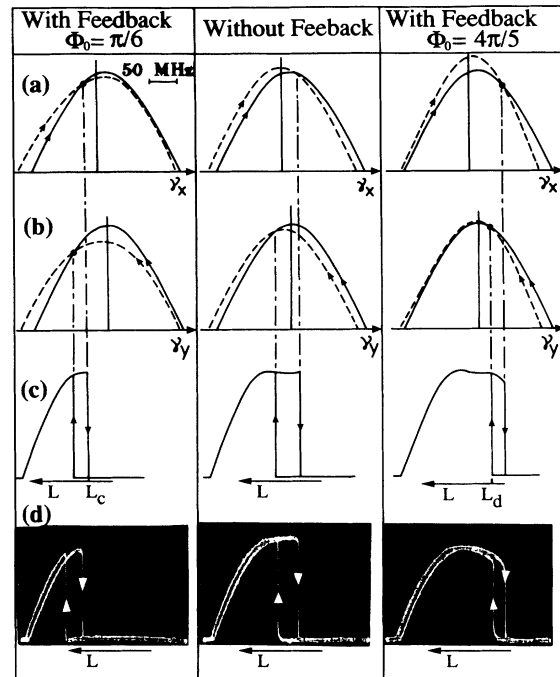


FIG. 22. Theoretical and experimental shifts of the hysteresis loop in the induced-inhibition mechanism for two values of the external parameter Φ_0 . The unperturbed hysteresis loop is used as reference. (a),(b) Representation of the flip conditions when the laser frequency increases and decreases, respectively. $\alpha_0 = 168 \times 10^6\text{ s}^{-1}$; $p = 94 \times 10^6\text{ s}^{-1}$; $C = 1.1$. (c),(d) Theoretical and experimental hysteresis loops. Output power I_x vs cavity length. (I_x axis, $3\mu\text{W}/\text{div}$; L axis, $50\text{MHz}/\text{div}$).

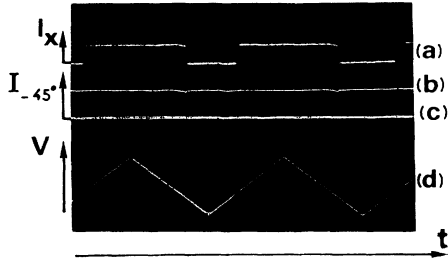


FIG. 23. Induced-inhibition gate. (a) Output I_x of the x eigenstate vs time. (I_x axis, $10 \mu\text{W}/\text{div}$; t axis, $10 \text{ms}/\text{div}$). (b) Output power with the polarizer P_y at -45° from the x axis (I_{-45° axis, $2.5 \mu\text{W}/\text{div}$; t axis, $10 \text{ms}/\text{div}$). (c) Zero intensity for I_{-45° . (d) Sawtooth voltage applied to the feedback piezoelectric transducer (V axis, $50 \text{V}/\text{div}$; t axis, $10 \text{ms}/\text{div}$).

is fixed at $\Delta\Phi_{xy} = 9^\circ$ and $a = 0.52$. The corresponding theoretical hysteresis loops in Fig. 22(c) show the existence of loop shifts when the phase Φ_0 varies. This is well verified by the experimental hysteresis loops in Fig. 22(d).

2. Optical gates

Let us define the maximum cavity length for the x -to- y flip by L_c and the minimum cavity length for the y -to- x flip by L_d [Fig. 22(c)]. When the laser cavity length is fixed between these two lengths we also obtain by varying the phase Φ_0 optical gates with high signal-to-noise ratios as shown in Fig. 23. There are no dips at the switching points when the polarizer P_y is rotated at 45° from the x eigenstate. So the anisotropic feedback induces the polarization flip following the inhibition mechanism. The switching energy in this process has been evaluated like for the rotation mechanism. By the measurement of the calibrated attenuation the switching energy must be increased by a factor of 25, leading to a 20-fJ switching energy.

So with an anisotropic feedback, i.e., in a one-frequency system, an external perturbation leads to a shift of the hysteresis domain allowing a polarization control following the induced-rotation and the induced-inhibition mechanisms. Optical gates with high signal-to-noise ratios are obtained with low switching energy.

IV. CONCLUSION

We have given a detailed description of the basic mechanisms, i.e., the rotation and the inhibition mechanisms, that occur in the polarization flipping of vectorial bistable quasi-isotropic lasers. We have pointed out the quite different properties of both processes. Indeed, the evolutions of the hysteresis loops versus laser frequency with phase anisotropy and laser excitation are opposed in these two processes. Additional evolutions of the polarization, such as multiple switchings, hybrid hysteresis loops, have been also isolated and understood in a gas laser. The polarization switchings occur in other quasi-isotropic lasers such as in semiconductor lasers. For instance, in a bistable semiconductor laser the bistability

between TE and TM modes is shown to be due to the inhibition mechanism. In fact, in general, it is the inhibition mechanism which appears the most frequently in vectorial bistable lasers, the rotation mechanism existing only for low anisotropy values. We have also investigated the optical control of vectorial bistabilities in a one-frequency system. A small injected signal by an anisotropic feedback controls the polarization both in *induced-rotation* and in *induced-inhibition* mechanisms. In contrast with most scalar bistable devices, in vectorial systems no energy is wasted during the flip. Indeed, there is only a shift of the energy from one to the other eigenstate. We obtain then optical gates with low switching energy especially in the induced-rotation mechanism with high signal-to-noise ratios. We have shown that for both descriptions of the basic mechanisms and of the polarization control by an anisotropic feedback the theoretical results are in good agreement with experiments.

ACKNOWLEDGMENTS

The authors are happy to thank Y. C. Chen and J. M. Liu for the semiconductor part and J. P. Taché and F. Bretenaker for their helpful discussions. This work was supported by the "Centre National de la Recherche Scientifique," the "Direction des Recherches, Etudes et Techniques," the "Pôle Optique et Optoélectronique de Formation des Ingénieurs par la Recherche Technologique" and the "Etablissement Public Régional." The Laboratoire d'Electronique Quantique is "Unité de Recherche Associée au CNRS No. 1202."

APPENDIX A

Here we calculate the losses $\Delta p(\theta)$ introduced by a frequency shift in the rotation mechanism. We suppose that for small anisotropy values the electric field remains in first step linearly polarized during the flip. At instant t the x component may be written as

$$E_x = E \cos(\theta) \exp(i2\pi\nu t). \quad (\text{A1})$$

Neglecting the shift of the frequency and the variation of θ for one round-trip in the laser cavity, the x component becomes

$$E'_x = E \cos(\theta) \exp[i(2\pi\nu t + \Phi_x)], \quad (\text{A2})$$

where the phase shift Φ_x of the x component from the resonance may be written as

$$\Phi_x = 2\pi(\nu - \nu_x)(2L/c). \quad (\text{A3})$$

We can deduce the losses Δp_x

$$\Delta p_x = [E \cos(\theta) - E \cos(\theta) \cos\Phi_x] / E \cos\theta, \quad (\text{A4})$$

which reduces, for small values of the phase Φ_x , to

$$\Delta p_x \approx \Phi_x^2 / 2. \quad (\text{A5})$$

With a similar method we derive the Δp_y losses on the y axis

$$\Delta p_y \approx \Phi_y^2 / 2, \quad (\text{A6})$$

where $\Phi_y = 2\pi(\nu - \nu_y)(2L/c)$. The total amplitude losses Δp are derived by noting that the total intensity $I = I_x + I_y$ after one round-trip becomes

$$I' = E^2(1 - \Delta p)^2 = (E \cos\theta)^2(1 - \Delta p_x)^2 + (E \sin\theta)^2(1 - \Delta p_y)^2. \quad (\text{A7})$$

As the losses $\Delta p_x, \Delta p_y$, and Δp are small, we deduce in first order

$$\Delta p(\theta) \approx \Delta p_x \cos^2\theta + \Delta p_y \sin^2\theta. \quad (\text{A8})$$

For simplification we assume that the phase shifts Φ_x and Φ_y vary linearly with θ , i.e.,

$$\Phi_x = -2\Delta\Phi_{xy}\theta/\pi/2 \quad \text{and} \quad \Phi_y = 2\Delta\Phi_{xy}(\pi/2 - \theta)/\pi/2. \quad (\text{A9})$$

Expressions (A5) and (A9) for Δp_x and (A6) and (A9) for Δp_y lead then to the following total losses for the field amplitude after a round-trip,

$$\Delta p(\theta) \approx 8\Delta\Phi_{xy}^2 [\theta^2 \cos^2(\theta) + (\pi/2 - \theta)^2 \sin^2\theta] / \pi^2. \quad (\text{A10})$$

APPENDIX B

In this appendix we derive the evolutions of the rotation angle θ of the main axis and of the ellipticity χ of an elliptically polarized field due to the active medium, to a linear phase anisotropy and to a loss anisotropy. We separate directly the contribution of the active medium from that of the two anisotropies.

1. Contribution of the active medium

The electric field \mathbf{E} can be defined in the circularly polarized basis (σ^+, σ^-) where $\sigma^\pm = 2^{-1/2}(\mathbf{x} \pm i\mathbf{y})$. For an isotropic cavity the evolutions of the amplitudes E_+ and E_- may be written [4] as

$$\dot{E}_+ = E_+(\alpha_+ - \beta_+ E_+^2 - \theta_{+-} E_-^2), \quad (\text{B1a})$$

$$\dot{E}_- = E_-(\alpha_- - \beta_- E_-^2 - \theta_{-+} E_+^2), \quad (\text{B1b})$$

where α_+ and α_- are the net gain coefficients and β_+, β_- and θ_{+-}, θ_{-+} the self- and cross-saturation coefficients. The angular frequency-determining equations are

$$\nu_+ + \dot{\Phi}_+ = \Omega + \sigma_+ - \rho_+ E_+^2 - \tau_{+-} E_-^2, \quad (\text{B2a})$$

$$\nu_- + \dot{\Phi}_- = \Omega + \sigma_- - \rho_- E_-^2 - \tau_{-+} E_+^2, \quad (\text{B2b})$$

where ν_+ and ν_- are the angular frequencies of the circularly polarized components, Φ_+ and Φ_- their phases, Ω is the angular resonant frequency of the empty cavity, σ_+ and σ_- are the linear pulling terms, and ρ_+, ρ_- and τ_{+-}, τ_{-+} are the self- and cross-pushing terms.

(a) Rotation of the main axis

The phase shift between the circular components induces a rotation whose evolution is written as

$$\dot{\theta} = \frac{1}{2}(\dot{\Phi}_- - \dot{\Phi}_+). \quad (\text{B3})$$

In our case there is no magnetic field, so $\nu_+ = \nu_-$ implying $\sigma_+ = \sigma_-$, $\rho_+ = \rho_-$, $\tau_{+-} = \tau_{-+}$. According to Eqs. (B2a) and (B2b), Eq. (B3) becomes

$$\dot{\theta} = \frac{1}{2}(\tau_{+-} - \rho_+) I \sin 2\chi, \quad (\text{B4})$$

where I is the total intensity defined by $I = E_+^2 + E_-^2 = I_+ + I_-$ and χ is the ellipticity defined by

$$\chi = \tan^{-1}(E_- - E_+) / (E_- + E_+) = \frac{1}{2} \sin^{-1}(I_- - I_+) / (I_- + I_+).$$

(b) Variation of the ellipticity

Time derivation of the first expression which defines χ leads to

$$\dot{\chi} = (E_+ \dot{E}_- - E_- \dot{E}_+) / I. \quad (\text{B5})$$

According to Eqs. (B1a) and (B1b), noting that $\alpha_+ = \alpha_-$, $\beta_+ = \beta_-$, $\theta_{+-} = \theta_{-+}$, and that $E_+ E_- = I \cos 2\chi$, the evolution of χ may be written as

$$\dot{\chi} = \frac{1}{4}(\theta_{+-} - \beta_+) I \sin 4\chi. \quad (\text{B6})$$

2. Contribution of the linear phase anisotropy

An elliptically polarized field can be defined either by the azimuth θ of the main axis and by the ellipticity χ or by the angle θ_0 (Fig. 24) defined by $\tan\theta_0 = b/a$, where a and b are the amplitudes of the field components along the x and y axes, and by the phase shift φ between the x and y components. The variables θ, χ, θ_0 , and φ are linked together by the following relations [50]:

$$\sin 2\chi = \sin(2\theta_0) \sin\varphi, \quad (\text{B7a})$$

$$\tan 2\chi = \sin(2\theta) \tan\varphi. \quad (\text{B7b})$$

When the elliptically polarized field passes through the linear phase anisotropy the phase shift increases by an amount $\Delta\Phi_{xy}$ leading to a variation of θ and χ .

(a) Rotation of the main axis

By elimination of χ between Eqs. (B7a) and (B7b) we obtain

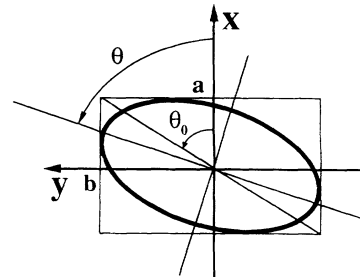


FIG. 24. Definition of the parameters θ, θ_0, a , and b for an elliptically polarized electric field.

$$\tan 2\theta = \tan(2\theta_0) \cos \varphi . \quad (\text{B8})$$

The differentiation of this equation, letting $d\varphi = \Delta\Phi_{xy}$, leads to

$$d\theta = -\frac{\Delta\Phi_{xy}}{2} \tan(2\theta_0) \cos^2(2\theta) \sin \varphi . \quad (\text{B9})$$

So according to Eqs. (B8) and (B7b) the time evolution of θ due to the phase anisotropy is

$$\dot{\theta} = -\frac{c}{L} \frac{\Delta\Phi_{xy}}{2} \tan(2\chi) \cos 2\theta . \quad (\text{B10})$$

(b) Variation of the ellipticity

Similarly, by differentiation of Eq. (B7a) one obtains

$$d\chi = \frac{\Delta\Phi_{xy}}{2} \sin(2\theta_0) \cos(\varphi) / \cos 2\chi , \quad (\text{B11})$$

and relations (B7a) and (B7b) lead then to the time evolution of the ellipticity

$$\dot{\chi} = \frac{c}{L} \frac{\Delta\Phi_{xy}}{2} \sin 2\theta . \quad (\text{B12})$$

3. Contribution of a loss anisotropy

We investigate now the effect of an x - y -type loss anisotropy introduced, for instance, by an intracavity tilted plate. The loss axes x and y are chosen to be parallel to those of the phase anisotropy $\Delta\Phi_{xy}$.

(a) Rotation of the main axis

Let us consider an elliptically polarized field with a small ellipticity. Then in first approximation the azimuth θ of the main axis can be defined by

$$\tan \theta \approx E_y / E_x . \quad (\text{B13})$$

After a passage of the vibration through the plate θ becomes θ' with

$$\tan \theta' = t_y E_y / t_x E_x , \quad (\text{B14})$$

where t_x and t_y are the x and y transmission coefficients of the tilted plate for the field amplitude. From Eqs. (B13) and (B14) we derive

$$\tan(\theta' - \theta) = (t_y / t_x - 1) \frac{\tan \theta}{1 + (t_y / t_x) \tan^2 \theta} . \quad (\text{B15})$$

As $t_y \approx t_x$ then $\theta' \approx \theta$ and the time behavior of θ due to the loss anisotropy may be written as

$$\dot{\theta} = \frac{c}{2L} (t_y / t_x - 1) \sin 2\theta . \quad (\text{B16})$$

(b) Evolution of the ellipticity

The differentiation of Eq. (B7b) leads to

$$d\chi = \cos^2(2\chi) \cos(2\theta) \tan \varphi d\theta . \quad (\text{B17})$$

According to the low ellipticity χ value we write

$\cos(2\chi) \approx 1$ and the time evolution of χ due to the loss anisotropy reduces to

$$\dot{\chi} = \cos(2\theta) \tan(\varphi) \dot{\theta} . \quad (\text{B18})$$

Insertion of Eqs. (B7b) and (B16) in (B18) leads then to

$$\dot{\chi} \approx \frac{c}{L} (t_y / t_x - 1) \chi \cos 2\theta . \quad (\text{B19})$$

We can note that for low ellipticity and loss anisotropy values the contribution of the loss anisotropy to $\dot{\chi}$ is negligible.

4. Total time evolution of θ and χ

As the phase and loss anisotropies are small, it is therefore possible to write $\dot{\theta}$ and $\dot{\chi}$ as the sum of the contributions of the active medium and of the phase and loss anisotropies. Then Eqs. (B4), (B10), and (B16) lead for low ellipticity values to

$$\dot{\theta} = (\tau_{+-} - \rho_{+-}) I \chi - \frac{c}{L} \Delta\Phi_{xy} \chi \cos 2\theta + \frac{c}{2L} (t_y / t_x - 1) \sin 2\theta , \quad (\text{B20})$$

and Eqs. (B6), (B12), and (B19) to

$$\begin{aligned} \dot{\chi} = & (\theta_{+-} - \beta_{+-}) I \chi + \frac{c}{L} \frac{\Delta\Phi_{xy}}{2} \sin 2\theta \\ & + \frac{c}{L} (t_y / t_x - 1) \chi \cos 2\theta . \end{aligned} \quad (\text{B21})$$

Equations (B20) and (B21) are in agreement with those obtained by van Haeringen [Ref. [10], Eqs. (13) and (14)] for low ellipticity values with $\theta_1 = \theta_2 = a' = \Phi' = H_z = 0$ and with $\beta_1 = 2\beta_+$, $\beta_2 = 2\theta_{+-}$, $\rho_1 = 2\rho_+$, $\rho_2 = 2\tau_{+-}$. The coefficient 2 is due to the fact that the vectors of the circularly polarized basis used by van Haeringen are not unitary.

APPENDIX C

From Eqs. (B20) and (B21) we deduce here the x -to- y flipping condition in the rotation mechanism. The coupled equations for $\dot{\theta}$ and $\dot{\chi}$ can, in general, be solved only by numerical integration. Approximate analytic solutions can, however, be obtained by assuming $\dot{I} = \dot{\chi} = 0$ [10]. Equations (B1a) and (B1b) lead to

$$I = E_+^2 + E_-^2 \approx 2\alpha_+ / (\beta_+ + \theta_{+-}) . \quad (\text{C1})$$

Letting $\dot{\chi} = 0$ we can deduce from Eqs. (B21) and (C1) for a low ellipticity value and neglecting the contribution of the loss anisotropy

$$\chi \approx -\frac{c}{L} \frac{1}{4\alpha_+} \frac{S+1}{2S} \Delta\Phi_{xy} \sin 2\theta , \quad (\text{C2})$$

where

$$\frac{S+1}{2S} = \frac{\theta_{+-} + \beta_+}{\theta_{+-} - \beta_+} .$$

For a $J=1 \rightarrow J=2$ transition $S = -\frac{3}{20}$ [10]. Insertion of (C2) in (B20) gives for a low anisotropy value

$$\dot{\theta} = \frac{c}{L} \sin(2\theta) \left[-\frac{1}{2} \frac{\rho_+}{\beta_+} \Delta\Phi_{xy} + \frac{c}{L} \frac{1}{4\alpha_+} \frac{S+1}{2S} \Delta\Phi_{xy}^2 \cos(2\theta) + \frac{1}{2} (t_y/t_x - 1) \right], \quad (C3)$$

where

$$\frac{\rho_+}{\beta_+} = \frac{\tau_{+-}}{\theta_{+-}} = \frac{\tau_{+-} - \rho_+}{\theta_{+-} - \beta_+}.$$

Let us consider a small rotation angle ϵ of the electric field from the stationary solution $\theta=0$ which corresponds to the x eigenstate. The expression (C3) becomes

$$\dot{\epsilon} = \frac{c}{L} 2\epsilon \left[-\frac{1}{2} \frac{\rho_+}{\beta_+} \Delta\Phi_{xy} + \frac{c}{L} \frac{1}{4\alpha_+} \frac{S+1}{2S} \Delta\Phi_{xy}^2 + \frac{1}{2} (t_y/t_x - 1) \right] + O(\epsilon^2), \quad (C4)$$

where $O(\epsilon^2)$ represents terms of the order of ϵ^2 which can be neglected for sufficiently small deviations from the x axis. The polarization flips from $\theta=0$ to $\theta=\pi/2$, i.e., from x to y , if ϵ builds up, that is if $\dot{\epsilon} > 0$. So the x -to- y flip condition may be written as

$$\left[-\frac{1}{2} \frac{\rho_+}{\beta_+} \Delta\Phi_{xy} \right] + \left[\frac{c}{L} \frac{1}{4\alpha_+} \frac{S+1}{2S} \Delta\Phi_{xy}^2 \right] + \frac{1}{2} [t_y/t_x - 1] > 0. \quad (C5)$$

The y -to- x flip condition derived in a similar fashion shows that only the signs of the first and third terms of (C5) are changed.

-
- [1] S. D. Smith, *Appl. Opt.* **25**, 1550 (1986); B. Rheinländer, A. Klehr, O. Ziemann, V. Gottschalch, and G. Oelgart, *Opt. Commun.* **80**, 259 (1991); Y. Ozeki and C. L. Tang, *Appl. Phys. Lett.* **58**, 2214 (1991); B. M. Yu and J. M. Liu, *J. Appl. Phys.* **69**, 7444 (1991).
- [2] P. W. Smith, *Bell. Syst. Tech. J.* **61**, 1975 (1982).
- [3] H. M. Gibbs, *Optical Bistability: Controlling Light with Light* (Academic, New York, 1985).
- [4] W. E. Lamb, Jr., *Phys. Rev.* **134**, A1429 (1964); M. Sargent III, M. O. Scully, and W. E. Lamb, Jr., *Laser Physics* (Addison-Wesley, Reading, MA, 1974).
- [5] B. van der Pol, *Philos. Mag.* **43**, 177 (1922); **43**, 700 (1922); **3**, 65 (1927).
- [6] See, for instance, R. L. Fork and M. A. Pollack, *Phys. Rev.* **139**, A1408 (1965).
- [7] W. Culshaw and J. Kannelaud, *Phys. Rev.* **141**, 228 (1966); J. Kannelaud and W. Culshaw, *ibid.* **141**, 237 (1966).
- [8] W. M. Doyle and M. B. White, *Phys. Rev. Lett.* **17**, 467 (1966).
- [9] H. de Lang, *Philips Res. Rep. Suppl.* **8**, 1 (1967).
- [10] W. van Haeringen, *Phys. Rev.* **158**, 256 (1967).
- [11] W. J. Tomlinson and R. L. Fork, *Phys. Rev.* **164**, 466 (1967).
- [12] Note that polarization bistability in passive systems has also been recently investigated. See, for instance, E. Giacobino, *Opt. Commun.* **56**, 249 (1985); C. Parigger, P. Hannaford, and W. J. Sandle, *Phys. Rev. A* **34**, 2058 (1986); J. Yumoto and K. Otsuka, *ibid.* **34**, 4445 (1986); A. Korpel and A. W. Lohmann, *Appl. Opt.* **25**, 1528 (1986).
- [13] L. Landau and E. Lifshitz, *Statistical Physics* (Pergamon, New York, 1958), Chap. 14.
- [14] A. Le Floch, G. Ropars, J. M. Lenormand, and R. Le Naour, *Phys. Rev. Lett.* **52**, 918 (1984).
- [15] H. de Lang, *Philips Res. Rep.* **19**, 429 (1964); *Philips Tech. Rev.* **32**, 190 (1971).
- [16] S. T. Hendow, R. W. Dunn, W. W. Chow, and J. G. Small, *Opt. Lett.* **7**, 356 (1982).
- [17] Y. Mitsuhashi, *J. Appl. Phys.* **53**, 9200 (1982).
- [18] G. Stéphan and D. Hugon, *Phys. Rev. Lett.* **55**, 703 (1985); G. Stéphan, A. D. May, R. E. Mueller, and B. Aïssaoui, *J. Opt. Soc. Am. B* **4**, 1276 (1987).
- [19] G. Ropars, A. Le Floch, and R. Le Naour, *Europhys. Lett.* **3**, 695 (1987).
- [20] Y. C. Chen and J. M. Liu, *Appl. Phys. Lett.* **46**, 16 (1985).
- [21] G. Ropars, A. Le Floch, G. Jézéquel, R. Le Naour, Y. C. Chen, and J. M. Liu, *IEEE J. Quantum Electron.* **QE-23**, 1027 (1987).
- [22] H. Haken, *Synergetics* (Springer, Berlin, 1978).
- [23] V. DeGiorgio and M. O. Scully, *Phys. Rev. A* **2**, 1170 (1970).
- [24] J. F. Scott, M. Sargent III, and C. D. Cantrell, *Opt. Commun.* **15**, 13 (1975).
- [25] R. C. Jones, *J. Opt. Soc. Am.* **31**, 488 (1941); **32**, 486 (1942); **37**, 107 (1947); **38**, 671 (1948).
- [26] A. Le Floch and R. Le Naour, *Phys. Rev. A* **4**, 290 (1971); G. Stéphan, R. Le Naour, and A. Le Floch, *ibid.* **17**, 733 (1978).
- [27] M. Sargent III, W. E. Lamb, Jr., and R. L. Fork, *Phys. Rev.* **164**, 436 (1967); **164**, 450 (1967).
- [28] F. Aronowitz and R. J. Collins, *J. Appl. Phys.* **41**, 130 (1970).
- [29] W. M. Doyle and M. B. White, *Appl. Phys. Lett.* **5**, 193 (1964).
- [30] P. Lett, W. Christian, Surendra Singh, and L. Mandel, *Phys. Rev. Lett.* **47**, 1892 (1981).
- [31] Note that recently these rotation and inhibition mechanisms have been investigated for the flip between an ordinary and an extraordinary eigenstate: F. Bretenaker and A. Le Floch, *IEEE J. Quantum Electron.* **QE-26**, 1451 (1990). These mechanisms have been also isolated for two circularly polarized eigenstates: J. C. Cotteverte, F. Bretenaker, and A. Le Floch, *Opt. Lett.* **16**, 572 (1991).
- [32] This discussion is similar to that of a Zeeman laser including a loss anisotropy. See, for instance, J. C. Cotteverte, F. Bretenaker, and A. Le Floch, *Opt. Commun.* **79**, 321 (1990); A. Le Floch and G. Stéphan, *Phys. Rev. A* **6**, 845 (1972).
- [33] F. Bretenaker and A. Le Floch, *Phys. Rev. A* **42**, 5561 (1990).
- [34] P. W. Smith and T. Hänsch, *Phys. Rev. Lett.* **26**, 740

- (1971).
- [35] C. Brechignac, R. Vetter, and P. R. Berman, *Phys. Rev. A* **17**, 1609 (1978).
- [36] W. R. Bennett, Jr., *Phys. Rev.* **126**, 580 (1962).
- [37] A. Dienes, *Phys. Rev.* **174**, 400 (1968); *IEEE J. Quantum Electron.* **QE-4**, 260 (1968).
- [38] J. C. Cotteverte, F. Bretenaker, and A. Le Floch, *Appl. Opt.* **30**, 305 (1991).
- [39] N. K. Dutta and D. C. Craft, *J. Appl. Phys.* **56**, 65 (1984).
- [40] N. K. Dutta, *J. Appl. Phys.* **55**, 285 (1984).
- [41] J. M. Liu and Y. C. Chen, *IEEE J. Quantum Electron.* **QE-21**, 271 (1985).
- [42] F. Bretenaker, A. Le Floch, J. Davit, and J. M. Chiquier, *IEEE J. Quantum Electron.* **28**, 348 (1992).
- [43] J. P. van der Ziel and R. M. Mikulyak, *IEEE J. Quantum Electron.* **QE-20**, 223 (1984).
- [44] E. M. Philipp-Rutz, *IEEE J. Quantum Electron.* **QE-14**, 112 (1978).
- [45] F. Favre, D. Le Guen, and J. C. Simon, *IEEE J. Quantum Electron.* **QE-18**, 1712 (1982).
- [46] Th. H. Peek, P. T. Bolwijn, and C. Th. J. Alkemade, *Am. J. Phys.* **35**, 820 (1967).
- [47] A. W. Lohmann, *Appl. Opt.* **25**, 1594 (1986).
- [48] For this evaluation we did not take into account the critical slowing down which we have found experimentally to be of the order of 10τ leading to a 8-fJ switching energy. For an outline of this phenomenon in scalar systems see, for instance, R. Bonifacio and P. Meystre, *Opt. Commun.* **29**, 131 (1979); E. Garmire, J. H. Marburger, S. D. Allen, and H. G. Winful, *Appl. Phys. Lett.* **34**, 374 (1979); S. Cribier, E. Giacobino, and G. Grynberg, *Opt. Commun.* **47**, 170 (1983).
- [49] W. F. Sharfin and M. Dagenais, *Appl. Phys. Lett.* **48**, 321 (1986).
- [50] M. Born and E. Wolf, *Principles of Optics* (Pergamon, New York, 1964), Chap. 1.

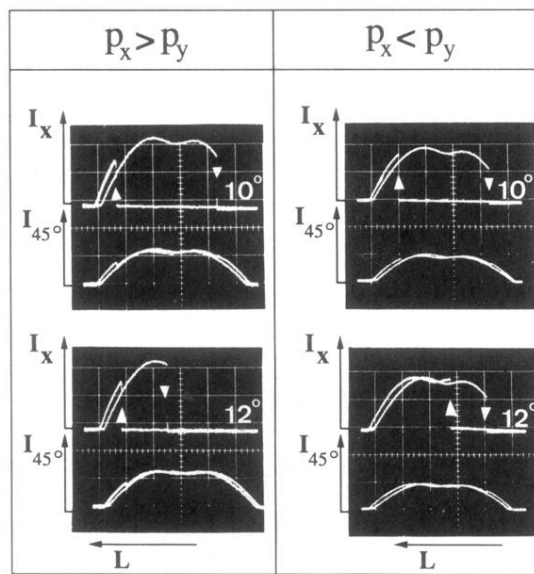


FIG. 10. Experimental evolution of the hysteresis loop with the phase anisotropy in the inhibition mechanism for low gas pressure (≈ 0.8 Torr). $p_x > p_y$. *Top*: $\Delta\Phi_{xy} = 10^\circ$. *Bottom*: $\Delta\Phi_{xy} = 12^\circ$. The hysteresis loop evolution is in agreement with the corresponding theoretical one [Fig. 9(c)]. $p_x < p_y$. *Top*: $\Delta\Phi_{xy} = 10^\circ$. *Bottom*: $\Delta\Phi_{xy} = 12^\circ$.

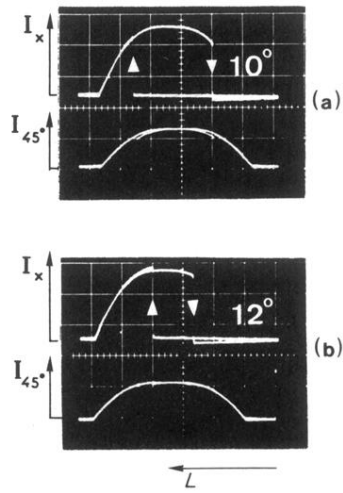


FIG. 11. Experimental evolution of the hysteresis loop with the phase anisotropy in the inhibition mechanism for high gas pressure (≈ 1.4 Torr). The hysteresis domain shrinks continuously. (a) $\Delta\Phi_{xy} = 10^\circ$. (b) $\Delta\Phi_{xy} = 12^\circ$.

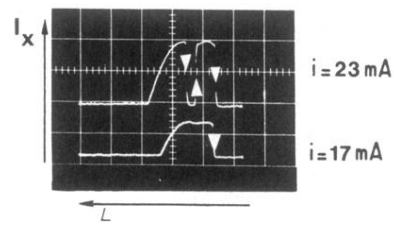


FIG. 13. Experimental results corresponding to the theoretical Fig. 12(c) for low gas pressure (≈ 0.6 Torr).

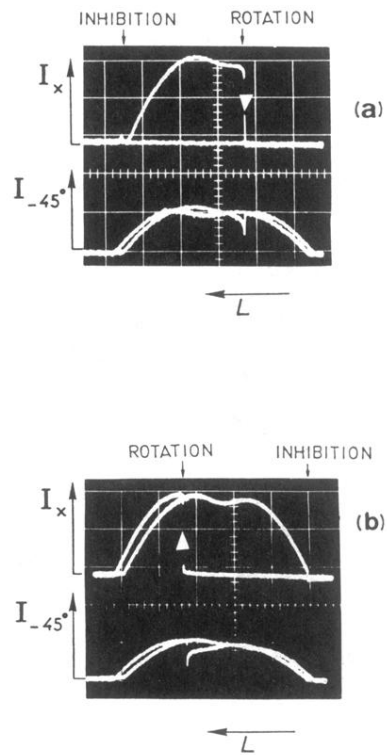


FIG. 15. Experimental hybrid hysteresis loop. (a) $p_x > p_y$. *Top*: hybrid bistable domain corresponding to Fig. 14(d). *Bottom*: polarizer at -45° from the x eigenstate allows to detect the two processes. (b) $p_x < p_y$. *Top*: hybrid bistable domain. *Bottom*: detection of the two mechanisms.

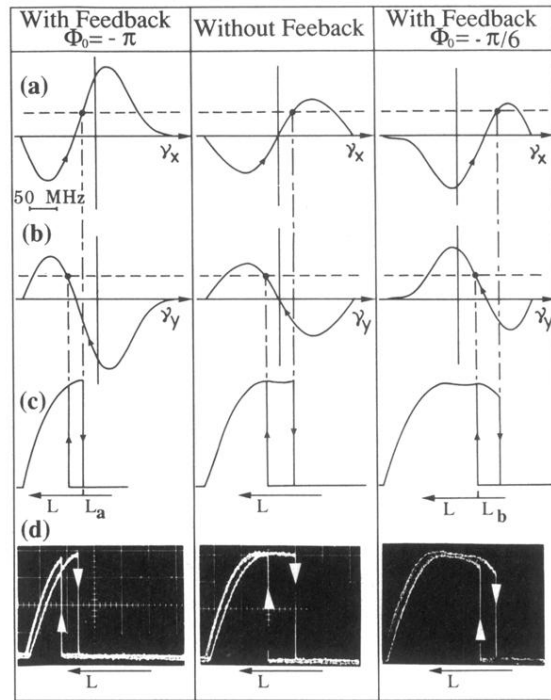


FIG. 19. Theoretical and experimental shifts of the hysteresis loop in the induced-rotation mechanism for two values of the external parameter Φ_0 . The unperturbed hysteresis loop is used as reference. (a),(b) Representation of the x -to- y and y -to- x flip conditions, respectively. $\alpha_0 = 168 \times 10^6 \text{ s}^{-1}$; $p = 94 \times 10^6 \text{ s}^{-1}$. (c),(d) Theoretical and experimental hysteresis loops. Output power I_x vs cavity length (I_x axis, $3\mu\text{W}/\text{div}$; L axis, $50 \text{ MHz}/\text{div}$).

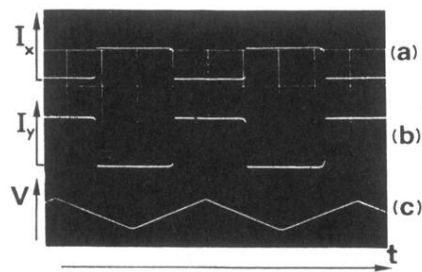


FIG. 20. Induced-rotation gate. (a) Output power I_x of the x eigenstate vs time (I_x axis, $10\mu\text{W}/\text{div}$; t axis, $10\text{ ms}/\text{div}$). (b) Output power I_y of the y eigenstate vs time (I_y axis, $10\mu\text{W}/\text{div}$; t axis, $10\text{ ms}/\text{div}$). (c) Sawtooth voltage applied to the feedback piezoelectric transducer (V axis, $50\text{ V}/\text{div}$; t axis, $10\text{ ms}/\text{div}$).

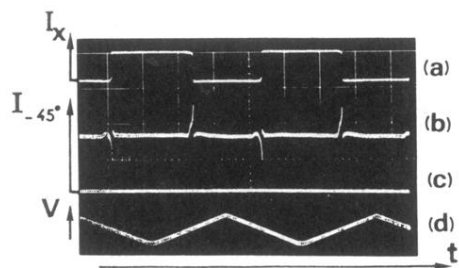


FIG. 21. Detection of the induced-rotation mechanism. (a) Same as in Fig. 21. (b) Output power with polarizer P_y at -45° from the x axis: induced-rotation dips and peaks are visible. (I_{-45° axis, $2.5 \mu\text{W}/\text{div}$; t axis, $10 \text{ ms}/\text{div}$). (c) Zero intensity for I_{-45° . (d) Same sawtooth voltage as in Fig. 20.

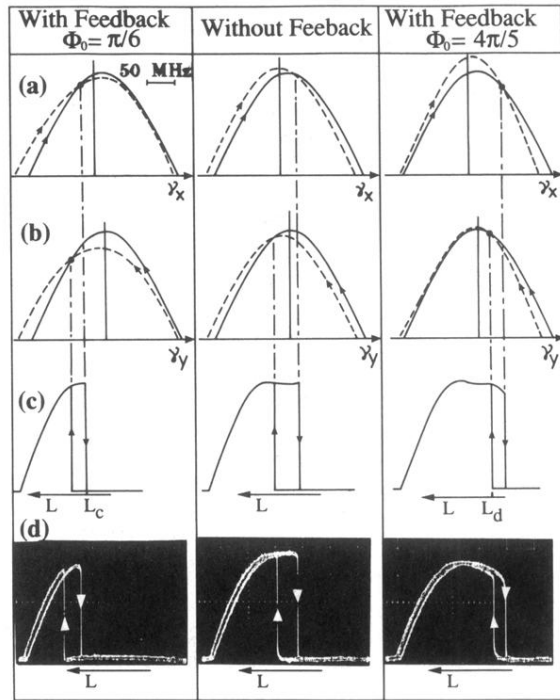


FIG. 22. Theoretical and experimental shifts of the hysteresis loop in the induced-inhibition mechanism for two values of the external parameter Φ_0 . The unperturbed hysteresis loop is used as reference. (a),(b) Representation of the flip conditions when the laser frequency increases and decreases, respectively. $\alpha_0 = 168 \times 10^6 \text{ s}^{-1}$; $p = 94 \times 10^6 \text{ s}^{-1}$; $C = 1.1$. (c),(d) Theoretical and experimental hysteresis loops. Output power I_x vs cavity length. (I_x axis, $3 \mu\text{W}/\text{div}$; L axis, $50 \text{ MHz}/\text{div}$).

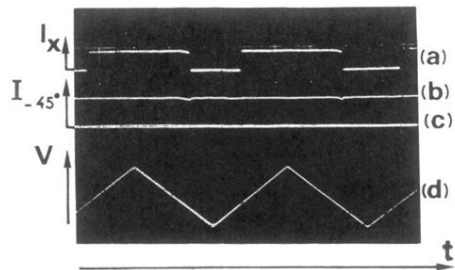


FIG. 23. Induced-inhibition gate. (a) Output I_x of the x eigenstate vs time. (I_x axis, $10 \mu\text{W}/\text{div}$; t axis, $10 \text{ms}/\text{div}$). (b) Output power with the polarizer P_y at -45° from the x axis (I_{-45° axis, $2.5 \mu\text{W}/\text{div}$; t axis, $10 \text{ms}/\text{div}$). (c) Zero intensity for I_{-45° . (d) Sawtooth voltage applied to the feedback piezoelectric transducer (V axis, $50 \text{V}/\text{div}$; t axis, $10 \text{ms}/\text{div}$).

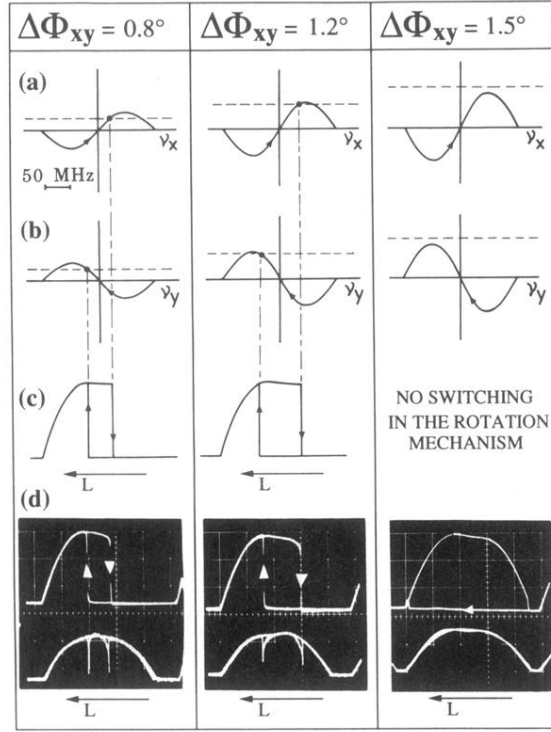


FIG. 5. Theoretical and experimental increase of the hysteresis loop with the phase anisotropy $\Delta\Phi_{xy}$ in the rotation mechanism. (a) Graphical resolution of the x -to- y flip condition (13). The arrows represent the frequency sweep direction. (b) Graphical resolution of the y -to- x flip condition. (c) Theoretical hysteresis loops. $\alpha_0 = 128 \times 10^6 \text{ s}^{-1}$; $p = 83 \times 10^6 \text{ s}^{-1}$ (the corresponding pump parameter is $\eta = 1.5$). (d) Experimental hysteresis loops. *Top*: the polarizer in front of the detector is along the x axis. The intensity on the x axis is I_x (I_x axis, $3\mu \text{ W/div}$; L axis, 60 MHz/div). *Bottom*: the polarizer in front of the detector is at 45° from the x axis. The dips show that the polarization flips following the rotating mechanism. Note that in (a) and (b) the horizontal axes represent the frequencies ν_x and ν_y , respectively, while in (c) and (d) the axes represent the experimental parameter, i.e., the cavity length L . The shift between the origins of the ν_x and ν_y frequency axes is proportional to $\Delta\Phi_{xy}$ and is here negligible.

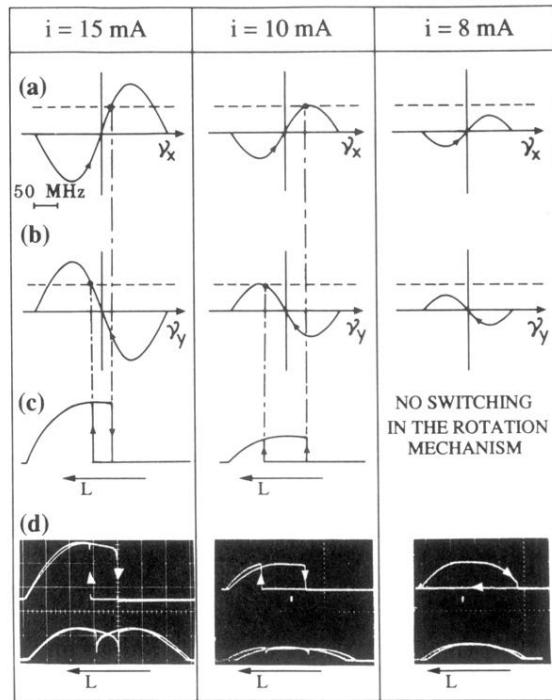


FIG. 6. Theoretical and experimental increase of the hysteresis loop when the current decreases in the rotation mechanism: (a)–(d) same as in Fig. 5. L axis: 50 MHz/div; $\alpha_0 = 158 \times 10^6 \text{ s}^{-1}$ for $i = 15 \text{ mA}$; $\alpha_0 = 128 \times 10^6 \text{ s}^{-1}$ for $i = 10 \text{ mA}$; $\alpha_0 = 111 \times 10^6 \text{ s}^{-1}$ for $i = 8 \text{ mA}$; $p = 83 \times 10^6 \text{ s}^{-1}$.

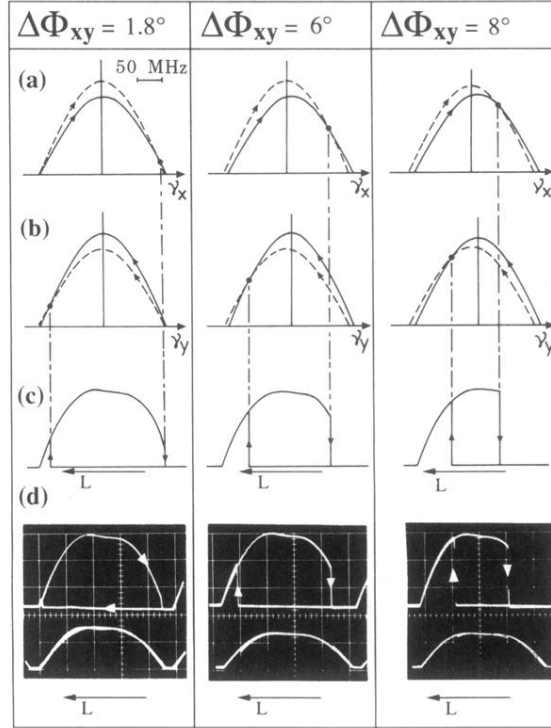


FIG. 7. Theoretical and experimental decrease of the hysteresis loop when the phase anisotropy $\Delta\Phi_{xy}$ increases in the inhibition mechanism. (a) Representation of the x -to- y flip condition. (b) Representation of the y -to- x flip condition. (c),(d) Theoretical and experimental hysteresis loops (I_x axis, 3μ W/div; L axis, 60 MHz/div). Note that for large values of $\Delta\Phi_{xy}$ the shift between the origins of the ν_x and ν_y frequency axes is noticeable. $\alpha_0 = 139 \times 10^6 \text{ s}^{-1}$; $C = 1.4$ for low anisotropy and 1.2 for 8° .

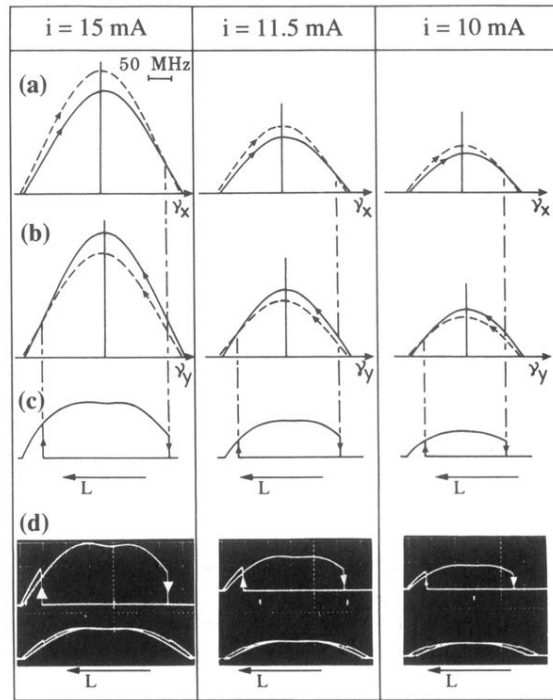


FIG. 8. Theoretical and experimental decrease of the hysteresis loop with the excitation current in the inhibition mechanism. (a)–(d) same as in Fig. 7. L axis: 50 MHz/div; $C = 1.4$; $\alpha_0 = 262 \times 10^6 \text{ s}^{-1}$ for $i = 15 \text{ mA}$; $\alpha_0 = 188 \times 10^6 \text{ s}^{-1}$ for $i = 11.5 \text{ mA}$; $\alpha_0 = 163 \times 10^6 \text{ s}^{-1}$ for $i = 10 \text{ mA}$; $p_x = p_y = 102 \times 10^6 \text{ s}^{-1}$.